IEEE Access
Multidisciplinary | Rapid Review | Open Access Journal

Received 16 August 2022, accepted 19 September 2022, date of publication 13 October 2022, date of current version 31 October 2022.

Digital Object Identifier 10.1109/ACCESS.2022.3214319

TOPICAL REVIEW

Review of Metasurfaces Through Unit Cell Design and Numerical Extraction of Parameters and Their Applications in Antennas

KOMAL IQBAL AND QASIM UMAR KHAN, (Member, IEEE)
Department of Electrical Engineering, College of Electrical and Mechanical Engineering, National University of Sciences and Technology, Islamabad 44000, Pakistan

Corresponding author: Qasim Umar Khan (qasimumar.khan@ceme.nust.edu.pk)

ABSTRACT A thorough review of metasurfaces (2D planar counterpart of metamaterials) based on electromagnetic (EM) classification i.e., ε-negative (ENG), μ-negative (MNG), and double-negative (DNG) materials is presented in this paper. The concept of left-handedness in metasurfaces which comprise of ENG, MNG, and DNG is demonstrated through basic Maxwell's equations. This concept is then explained by designing unit cells of each category along with numerical extractions of parameters through Kramers-Kronig rule (for ENG) and Nicholson-Ross-Weir (NRW for MNG and DNG), thereby verifying unit cell designs. This helps the reader to have complete insight regarding the design, simulation, and mathematical verification of ENG, MNG, and DNG-based metasurfaces used in antenna applications for gain enhancement, absorbers to reduce radar cross-section and beam forming. Moreover, the paper also provides a thorough review of the state-of-the-art research based on these metasurfaces in antenna applications delineated above. A comparison of the state of the art is drawn at the end of this review.

INDEX TERMS Metamaterials, negative refractive index materials, metasurface antennas, lens, gain enhancement, beam forming, and beam scanning.

I. INTRODUCTION

In 1999, the word "Metamaterial" was first coined by Walser who interpreted metamaterials as the fabricated 3-dimensional periodic structures synthesized to produce materials having exotic properties, which are not occupied by the materials present in nature [1]. Afterward, it was then appeared in the literature in 2000 [2]. Generally, metamaterials are the periodic arrangement of man-made structures having a size much smaller than the operating wavelength.

On the other hand, metasurfaces are the 2D correspondents of metamaterials. This type of ultra-thin and 2D structure serves to mitigate undesirable losses and strong dispersions in wave-propagation and is suitable for easy fabrication of micro and nano-structures [3].

The classification of metamaterials is based on the constitutive parameter values i.e., double-positive (DPS) in which both μ and ε are positive, ε-negative (ENG) μ-negative (MNG), and double negative (DNG) [4], [5], [6], [7]. Among these categories, dielectrics, magnetic materials, and plasmas are materials that exist in nature with DPS, MNG, and ENG values, respectively. But a DNG material does not exist in nature and has been engineered for production [8]. In this regard, Veselago published the first study on the properties of materials with negative permittivity and permeability simultaneously in [9]. Since then, this technology has been experimentally demonstrated in different forms for many applications with unique modifications. The initial DNG structure which was based on a 3D cylindrical Split-Ring-Resonator for DNG media and an array of metallic cylinders for ENG media was originally developed by Pendry et al., in [14]. However, the proposed structure wasn't applicable for 2D planar structures and exhibited non-isotropic properties (showing null magnetic response in other directions) including the flow of current that occurs along the length of the cylinders which is undesirable [88]. Therefore, the need for periodic and packed array structures emerged replacing cylindrical structures to prevent continuous

The associate editor coordinating the review of this manuscript and approving it for publication was Hassan Tariq Chattha.

conduction path. Hence, the split ring resonators (SRRs) and thin-wire strips with flat 2D structures were incepted. In this perspective, Schultz and co-workers experimentally demonstrated the properties of materials with a negative refractive index (NRI) using periodically implemented metal lines and SRRs [2], [15], [16], [17]. Although the designs in [2], [15], [16], and [17] solve the problem of an-isotropy, but these designs have large sizes and are not suitable for metasurfaces (i.e., 2D planar structures), as they cause problems in the fabrication.

To tackle the issue of size reduction, new structures based on SRRs and CSRRs (complementary SRRs) were introduced in [18], [19], [20], [21], [22], and [23]. The designs are useful for 2D metasurface due to size miniaturization and planar structure. Based on electromagnetic classifications, a series of research publications discussed ENG and MNG materials [24], [25], [26], [27], [28], [29], [30], [31], [32], [33], [34], [35], [36], [37], which are being applied in antenna's gain enhancement [24], micro-wave sensors [25], [26] metamaterial structures with multi-band characteristics [27], [28], [29], [30], [31], [32], [33], [34], wide-band metamaterial antennas [34]. and miniaturized zeroth-order resonance antenna [35], [37]. Similarly, number of research publications also discussed DNG properties having negative refractive index [38], [39], [40], [41], [42], [43], [44], [45], [46], [47], [48] which are used for variety of applications like super lenses [39], [40], biomedical field [41], [42], absorber metamaterial antennas [43], [44], [45] invisibility cloaks [46], enhanced focusing [47], [48], backward wave antennas [49], frequency reconfiguration [50], photon tunnelling [51], [52], [53], miniaturized DNG ZOR antennas (i.e., complementary right left-handed transmission line antenna, CRLH TL) [54], [55], [56], [57], [58]. The current research is also putting focus on the designing of SRRs applicable for 5G wireless communication [41], [58], [59], [60], [61], [62], [63], [64], [65], [66], [67]. The main problem associated with negative refractive index metamaterials is that they have narrow bandwidth and high dispersion losses. In this regard, [68], [69], [70], [71] were reported to design wide-band metamaterials, but none of these had addressed losses and radiation performance. To address these problems, the research is now shifted towards metasurface-based antennas, having potential applications in gain enhancement along with size miniaturization [72], [73], [74], [75] and wide bandwidth miniaturized MTS antennas [76], [77], [78], [79]. Moreover, based on the electromagnetic classification properties (i.e., ENG, MNG and DNG), metasurface antennas are being catered for gain and directivity enhancement [72], [73], [74], [75], [95], [96], [98], lens applications [80], [81], [82], [83], [84], [85], [86], [87], and perfect absorbers [88], [89], [90].

The objective of this paper is to provide the readers with a comprehensive overview about the basic electromagnetic classifications of metasurfaces by designing the unit cell of each classification and verifying these through simulation and mathematically by parameter extraction. The state-of-the-art research will be reviewed based on the classification and their potential applications.

The paper is organized as follows, metasurfaces are classified based on ε and μ values in Section I. For each classification, the metasurface based unit cell is designed, simulated, and numerical extraction of the parameters is carried out in Section II to give readers a comprehensive understanding of the designing process and parameters extraction of metasurfaces. Afterward, the state-of-the-art is discussed based on classified metasurfaces and their potential applications, especially in antenna designs in Section III. In the end, the conclusion and recommendations are provided in Section IV.

II. CLASSIFICATION OF METASURFACES

As discussed above, electromagnetic properties of materials are classified based on constitutive parameters i.e., permittivity (ε) and permeability (μ), which produce ENG, MNG, and DNG materials [4], [5], [6], [7]. The relationship between the refractive index 'n' and the constituent parameters ε and μ is given by the formula in [5]:

$$n = \pm\sqrt{\varepsilon\mu} \tag{1}$$

As shown in Fig.1, the electromagnetic metamaterials/metasurfaces are classified based on the values of ε and μ in different quadrants.

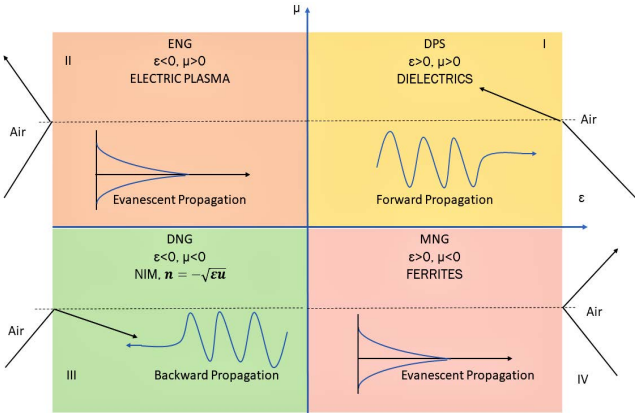

FIGURE 1. The classification of electromagnetic metamaterials/metasurfaces [5] @ IntechOp.

Fig. 1 demonstrates that in quadrant I, both ε and μ are positive forming a double-positive structure (DPS) or right-handed medium (RHM) which are easily found in nature such as dielectric materials in which EM waves can propagate. While in quadrant II, ε is negative and μ is positive, composing ENG i.e., epsilon negative medium which has properties like electric plasma. On the other hand, in quadrant III, both ε and μ are negative giving a double negative (DNG) or left-handed medium (LHM) which are not found in nature. The quadrant IV contains negative μ and positive ε, representing mu-negative (MNG) media, such as ferrite materials. From Fig.1, it is evident that waves can propagate in two media

lying in regions I and III, while the non-propagating evanescent waves are found in regions II and IV. The ambiguity of how these waves travel backward in a left-handed medium is cleared well by Maxwell's equations. For this purpose, consider the fundamental equations as given in [5].

$$\nabla \times \bar{E} = -j\omega\mu\bar{H} - \bar{M}_s \tag{2a}$$
$$\nabla \times \bar{H} = j\omega\varepsilon\bar{E} + \bar{J}_s \tag{2b}$$

where $\bar{E}$ and $\bar{H}$ are electric and magnetic field vectors, while $\bar{M}_s$ is the magnetic current density and J_s is the electric current density. Considering a plane wave, the electric ($\bar{E}$) and magnetic ($\bar{H}$) field vectors are represented as:

$$\bar{E} = \bar{E}_0 e^{-j\bar{\beta}\cdot\vec{a}} \tag{3}$$
$$\bar{H} = \bar{E}_0/\eta e^{-j\bar{\beta}\cdot\vec{a}} \tag{4}$$

where $\bar{\beta}$ is wave propagation constant and $\vec{a}$ is the decay constant, while η is the intrinsic impedance.

Now the information about the medium can be directly obtained by substituting the relations (3) and (4) into (1) and (2) respectively. For simplicity, consider source-free regions where $\bar{M}_s = J_s = 0$. Hence, after differentiation the response for the right-handed medium (where ε, μ >0) is as follows:

$$\bar{\beta} \times \bar{E} = +\omega\mu\bar{H} \tag{5a}$$
$$\bar{\beta} \times \bar{H} = -\omega\varepsilon\bar{E} \tag{5b}$$

On the other hand, for the case of a left-handed medium (where ε, μ <0), therefore the left-handed triplet would be as follow:

$$\bar{\beta} \times \bar{E} = -\omega|\mu|\bar{H} \tag{6a}$$
$$\bar{\beta} \times \bar{H} = +\omega|\varepsilon|\bar{E} \tag{6b}$$

The magnitudes of ε and μ are used to cater for the sign convention in the third quadrant. The relations in (5) and (6) form right-handed and left-handed triplets ($\bar{E}, \bar{H}, \bar{\beta}$), where $\bar{\beta}$ is the phase constant or wavenumber i.e., $k = \frac{2\pi}{\lambda} = \beta$.

Fig. 2 shows the response of right-handed and left-handed triplets in terms of pointing vector S, which determines energy flow response in terms of $\bar{E}$ and $\bar{H}$ vectors as follow:

$$S = {}^1\!/_2\bar{E} \times \bar{H}* \tag{7}$$

As the frequency is always positive, hence the response of phase velocity v_p determines that either the medium is right-handed or left-handed, by the following relation:

$$\bar{v_p} = \frac{\omega}{\beta}\hat{\beta} \text{ (where } \hat{\beta} = \bar{\beta}/|ß|) \tag{8}$$

Relation (8) shows that, for right-handed medium, relation (5) is in-phase with phase velocity which is dependent on phase response $\bar{\beta}$, while for the left-handed medium, relation (6) is out of phase with phase velocity. Hence $\bar{\beta}$ is the factor to decide the response for both mediums i.e.,

$$\beta > 0, v_p > 0 \text{----for RH} - \text{medium}$$
$$\&\beta < 0, v_p < 0 \text{----for LH} - \text{medium}$$

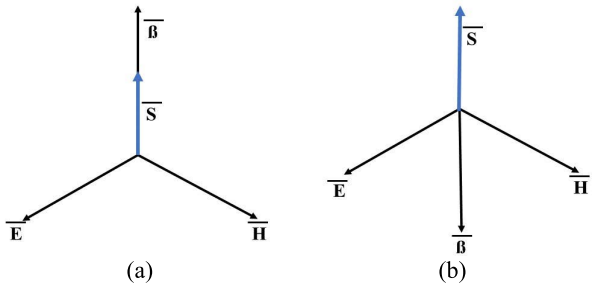

FIGURE 2. Right-handed medium (a), Left-handed medium (b) [5] @ IntechOpen.

TABLE 1. Parameters of ENG unit cell.

Parameters	Value (mm)
R	3.375
Sw	4.65
H, Hs	7
W,L	7
Ws	2.5

This antiparallel phase response can be better demonstrated by the generic phase lag and lead concept of a wave. Fig. 3(a) shows that the phase of wave 5 lags behind the phase of wave 1 with respect to time, thus the progression of the wave in a forward direction with a lagging (or positive) phase response establishes a right-handed medium. As both β and v_p is positive in this case, therefore according to the relation (8), both are parallel to each other. On the other hand, Fig. 3(b) shows that the phase of wave 5 leads the phase of wave 1 with respect to time, and develops a left-handed medium as the wave moves in a forward direction with a leading (or negative) phase response, as making $\bar{v_p}$ negative also, according to relation (8). Thus, the wave is traveling in the forward direction with negation phase velocity, producing an anti-parallel phase response. This notion is demonstrated in Fig.3 [6].

The combined effect of a group of waves traveling in the forward direction is demonstrated in Fig.4, by the parallel and antiparallel phases between phase velocity $\bar{v_p}$ and group velocity $\bar{v_g}$ (envelope), for right-handed and left-handed medium respectively.

This concludes that for left-handed medium, phase velocity $\bar{v_p}$ is anti-parallel to group velocity $\bar{v_g}$ with phase advance of propagating wave. Moreover, in terms of wave number k_n i.e.,

$$\beta = k_n = nk_0 = n\frac{\omega}{c} \tag{9}$$

where

$$n = \pm\sqrt{\varepsilon\mu} \tag{10}$$

The LH-medium contains $\beta < 0$, n is must less than 0 forming a negative refractive index with properties having negative ε_r *and* μ_r [6]. Based on these classifications, the next section demonstrates the ENG, MNG, and DNG effect through unit cell design simulations along with the verification of results

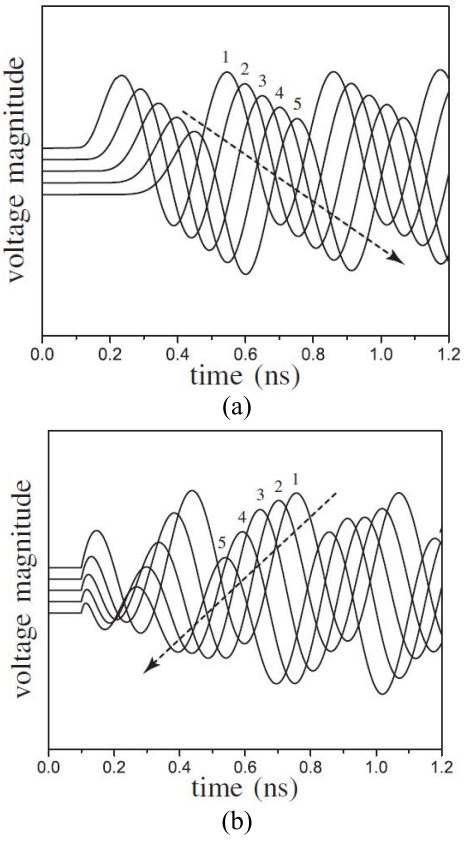

FIGURE 3. Wave propagation for (a) Right-handed medium with phase lag response for $\bar{v_p} > 0$, while (b) Left-handed medium with phase advance for $\bar{v_p} < 0$ [6] @ wiley.

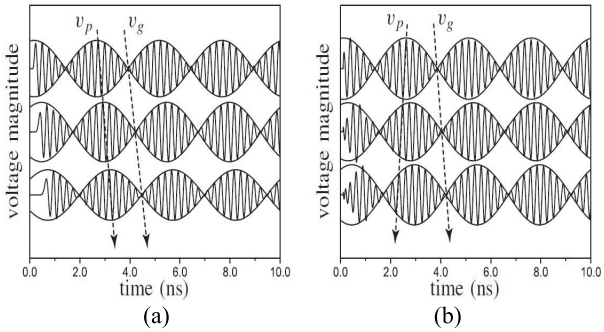

FIGURE 4. Propagation of wave with $\bar{v_p} > 0$ and $\bar{v_g} > 0$ for right-handed medium (a), and $\bar{v_p} < 0$ but $\bar{v_g} > 0$ for left-handed medium (b) [6] @ wiley.

through mathematical extraction of the parameters. This is done so that the readers may be provided with the basic information regarding the unit cell design and parametric extraction both using simulation and mathematics in the single platform. This will further help the readers to understand the state of the art which is presented in Section III.

III. ILLUSTRATING THE CLASSIFICATION BY DESIGNING UNIT CELLS

A. ENG BASED METASURFACE

It is demonstrated in the literature that ENG metamaterial is produced by using the metallic mesh of thin cylindrical wires

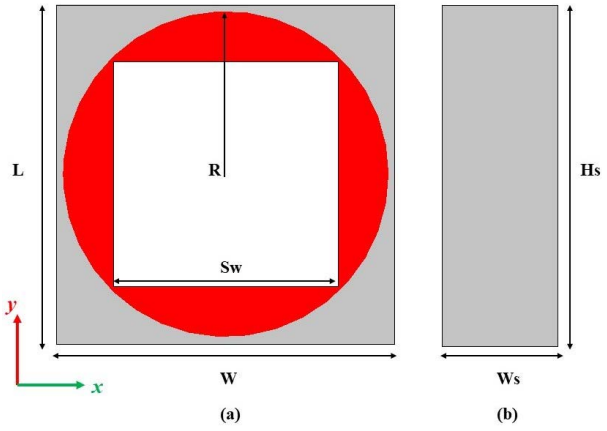

FIGURE 5. Geometry of proposed unit cell. (a) Front view, (b) Side view.

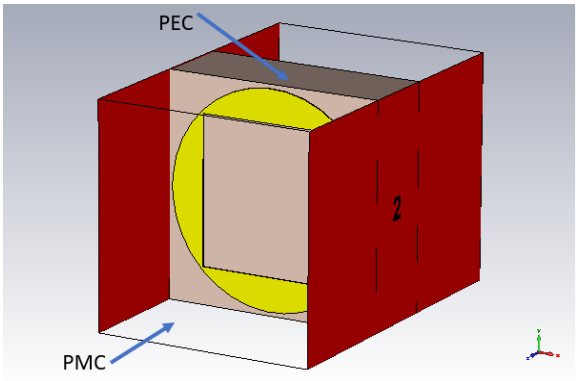

FIGURE 6. CST Model of ENG based metasurface unit cell.

TABLE 2. Parameters of MNG unit cell.

Parameters	Size (mm)	Parameters	Size (mm)
r1	1.8	g	0.1
r2	2.4	d	0.2
c	0.4	L	6
Ws	1.575	Ls	6
t(thickness of metal)	0.035	-	-

for obtaining a negative value of ε [7]. However, this thin cylindrical wire-media is not being applicable for 2D metasurface structures. Therefore, a new unit cell is designed to get negative epsilon value at the desired resonance frequency (6.2 GHz) to produce a 2D ENG metasurface. The designed unit cell structure is depicted in Fig.5, and its parameters are given in Table 1. It should be noted here that any other resonance frequency may be selected for unit cell design. For illustration purposes, the authors are using 6.2 GHz.

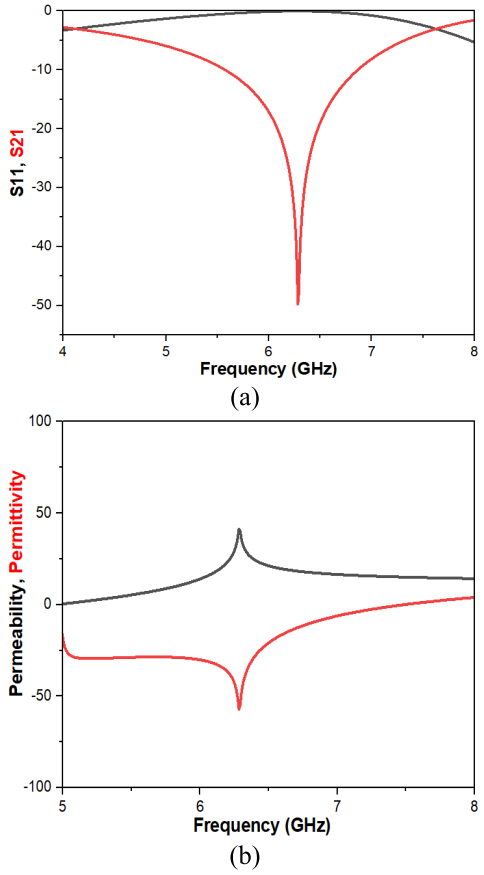

FIGURE 7. ENG-based Unit Cell, (a) S-parameters, (b) ε and μ results.

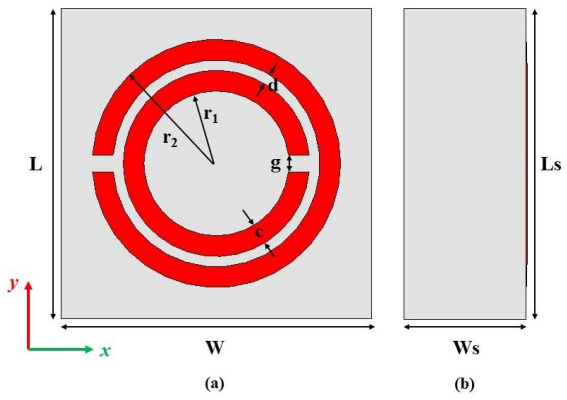

FIGURE 8. Geometry of the unit cell. (a) Front view, (b) Side view.

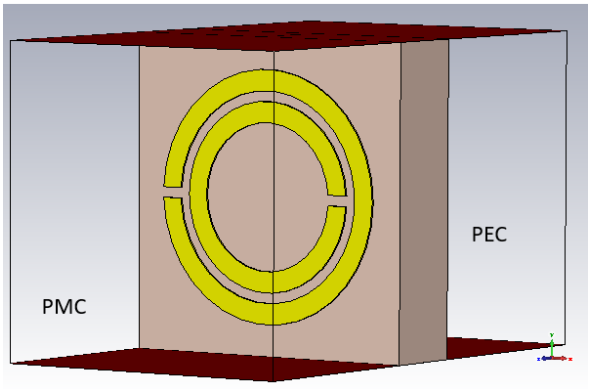

FIGURE 9. CST Model of MNG unit cell.

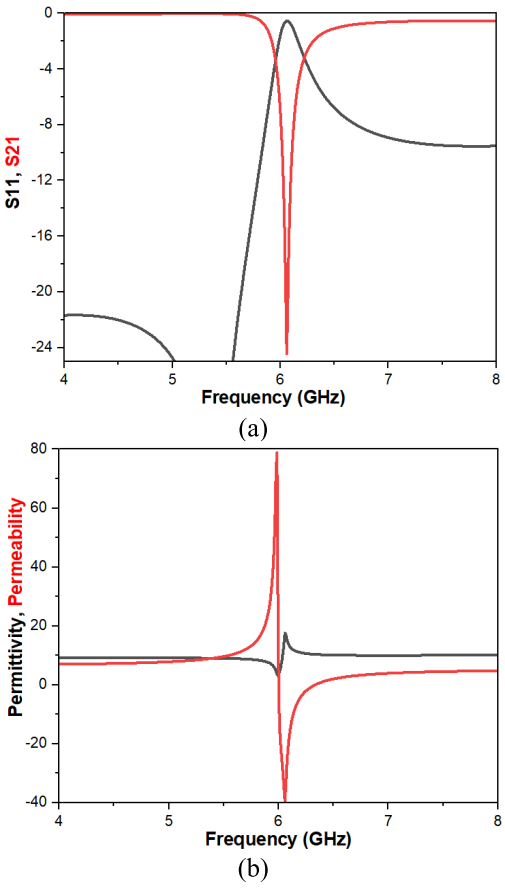

FIGURE 10. MNG-based Unit Cell. (a) S-parameters, (b) ε and μ results.

The designed structure contains a circular patch having radius R with a square slot of dimension d x d, and an Alumina substrate ($\varepsilon = 9.9$ and $\tan\delta = 0.0001$). If we consider an array of this unit cell, then below a cut-off frequency of the array there is no propagation, and an electromagnetic wave will experience total reflection. This behavior is similar to the propagation of the electromagnetic waves in plasma. If a lattice constant 'a' (i.e., the distance between unit cells) is much smaller than a wavelength ($a \ll \lambda$), the array structure can be thought of as a continuous plasma like material described by an effective permeability ε_{eff} in [7] as:

$$\varepsilon_{eff} = 1 - \frac{f_p^2}{f^2} \tag{11}$$

where fp the plasma frequency and f is the resonant frequency. To design a unit cell at a resonance frequency of 6.2 GHz, the condition $f_p > f$ must be fulfilled to keep permittivity negative. The equation relating f_p and design

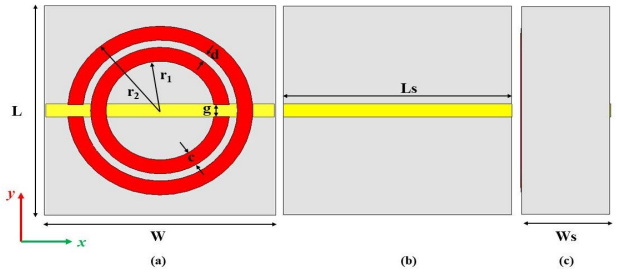

FIGURE 11. Unit cell's geometry. (a) Front-, (b) Back-, (c) Side-view.

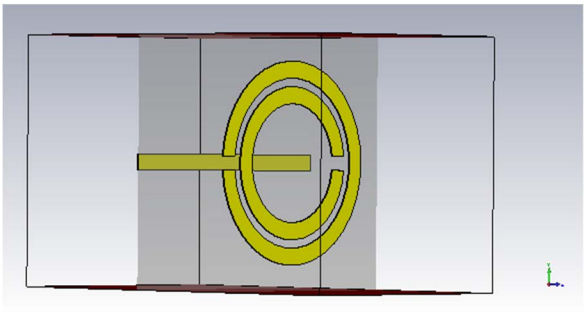

FIGURE 12. CST Model of DNG unit cell.

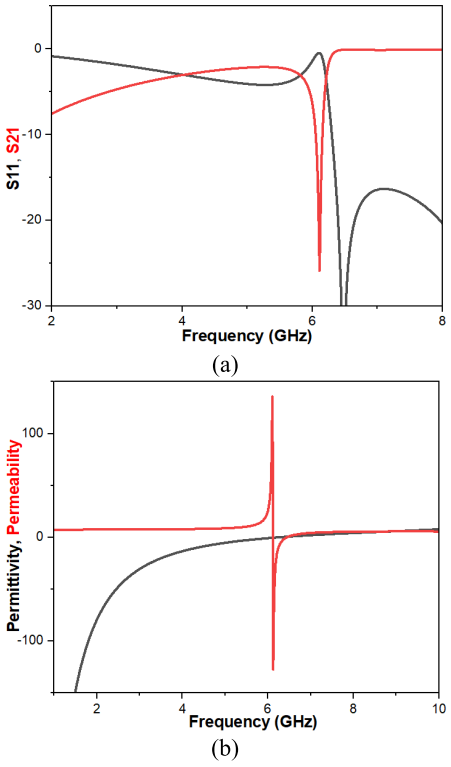

FIGURE 13. DNG-based Unit Cell. (a) S-parameters, (b) ε and μ results.

parameters are given in [91] as:

$$\omega_p^2 = \frac{2\pi c_0^2}{a^2 ln(a/r)} \tag{12}$$

TABLE 3. Parameters of DNG unit cell.

Parameters	Size (mm)	Parameters	Size (mm)
r1	1.8	g	0.165
r2	2.4	d	0.2
c	0.4	W,L, Ls	6
Ws	2.35	S	0.375

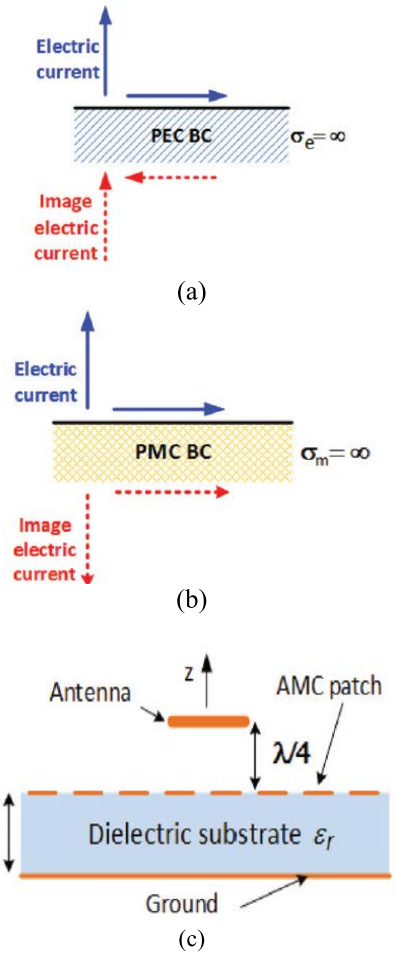

FIGURE 14. (a) Image currents due to PEC (b) and due to AMC (c) Theoretical model of antenna located above AMC loaded metasurface [1] @IEEE.

where a is the lattice constant and r is the radius of a circle. In the proposed design, the radius is 3.375 mm, while the lattice constant a should be 7mm to get $f_p > f$.

The cell is designed using a CST simulator to achieve desired results. The boundary conditions i.e., PEC and PMC are defined in the y- and z- directions respectively, as shown in Fig.6.

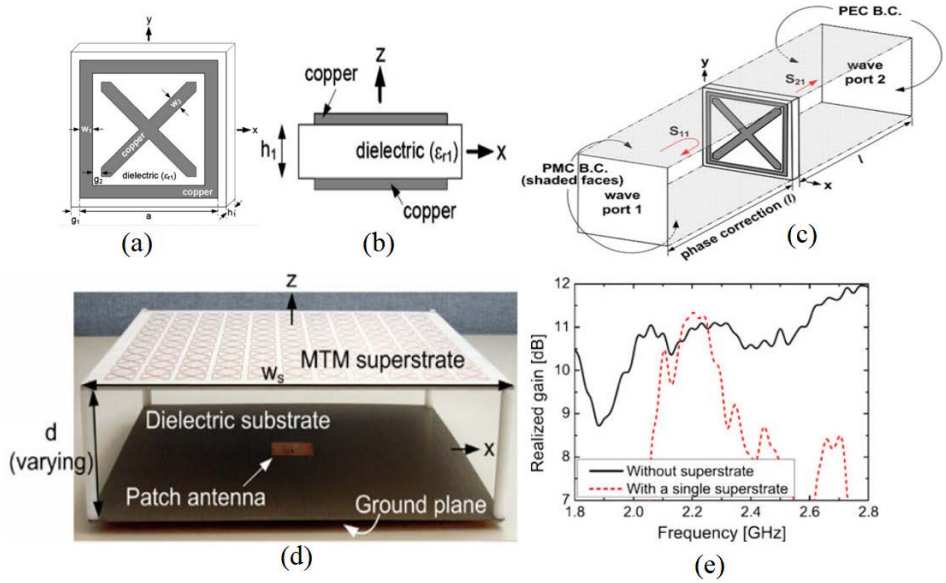

FIGURE 15. (a) Unit cell of Fabry-Pérot cavity model. (b) Side-view. (c) Boundary condition set-up. (d) Antenna's experimental set-up. (e) Measured realized gain. [96] @Springer.

1) RESULTS AND DISCUSSION

Fig. 7 shows the simulated S-parameters, ε, and μ results. The designed unit cell exhibits ENG properties with a negative ε value and positive μ value at the resonance frequency. Now to verify these characteristics, Kramers-Kronig relations [92] are utilized to extract the effective relative permittivity (ε), and permeability (μ) with the following relations:

$$z_{eff} = \pm\sqrt{\frac{(1+S_{11})^2 + S_{21}^2}{(1-S_{11})^2 - S_{21}^2}} \tag{13}$$

$$R_{01} = \frac{z_{eff}+1}{z_{eff}-1} \tag{14}$$

$$e^{in_{eff}k_0d_{eff}} = \frac{S_{21}}{1-S_{11}R_{01}} \tag{15}$$

$$n_{eff} = \frac{1}{k_0 d_{eff}} Im[ln(e^{in_{eff}k_0d_{eff}})] + 2\pi m - iRe[n(e^{in_{eff}k_0d_{eff}})]\} \tag{16}$$

$$\varepsilon_{eff} = \frac{n_{eff}}{z_{eff}} \& \mu_{eff} = n_{eff} z_{eff} \tag{17}$$

Where m is an integer denoting the branch index of a complex logarithm, i.e., m=0,1,2…, (keep it zero for the initial branch), d_{eff} is the thickness of the unit cell, k_0 is the wavenumber. Using the equations (13)- (17), the calculated values of ε and μ comes out as, −59.46 and 79.1 respectively, which are close to simulated results, i.e., −57.06 and 40.73.

B. MNG BASED METASURFACES

For the mu-negative (MNG) structure, the split ring cylindrical model is presented in [14]. But due to its non-isotropic behavior and flow of current along the length of the cylinder, the design was modified as a disc-like SRR suitable for planar applications [18], [19], [20], [21], [22], [23]. In this section, a unit cell of the SRR consisting of two concentric metallic rings, separated by a gap g is designed. The structure is designed using Rogers RT 5870 substrate ($\varepsilon = 2.33$ and tan $\delta = 0.0012$). The geometry of the unit cell and its designed model in CST are shown in Fig.8 and Fig.9, respectively. While all the parameters are mentioned in Table 2.

To design SRR at the desired frequency, the following relation is used [93]:

$$f_0 = \frac{1}{2\pi\sqrt{LC}} \tag{18}$$

The inductance of the ring can be calculated using the following relation [93]:

$$L = \mu_0 R_m \left(\ln\frac{8R_m}{t+c} - 0.5\right) \tag{19}$$

where $R_m = r1 + c/2$, t is the thickness of copper, c is the width of circular rings, and μ_0 is free space permeability. In this model, the total capacitance is the sum of gap capacitance C_{gap} and surface capacitance C_{sur}. Now to find C_{gap}, and C_{sur} following equations will be used [93]:

$$C_{gap} = \varepsilon_0[\frac{ct}{g} + \frac{2\pi}{ln(\frac{2.4t}{c})}] \tag{20}$$

$$C_{sur} = \frac{2\varepsilon_0 t}{\pi} ln\frac{4r1}{g} \tag{21}$$

where g is the cut slots of circular rings.

After getting the values of C_{gap} and C_{sur}, the split ring resonator can be designed at the desired resonance frequency by relation (18). For this model, the boundary conditions i.e., PEC and PMC are applied in the x- and z- directions respectively.

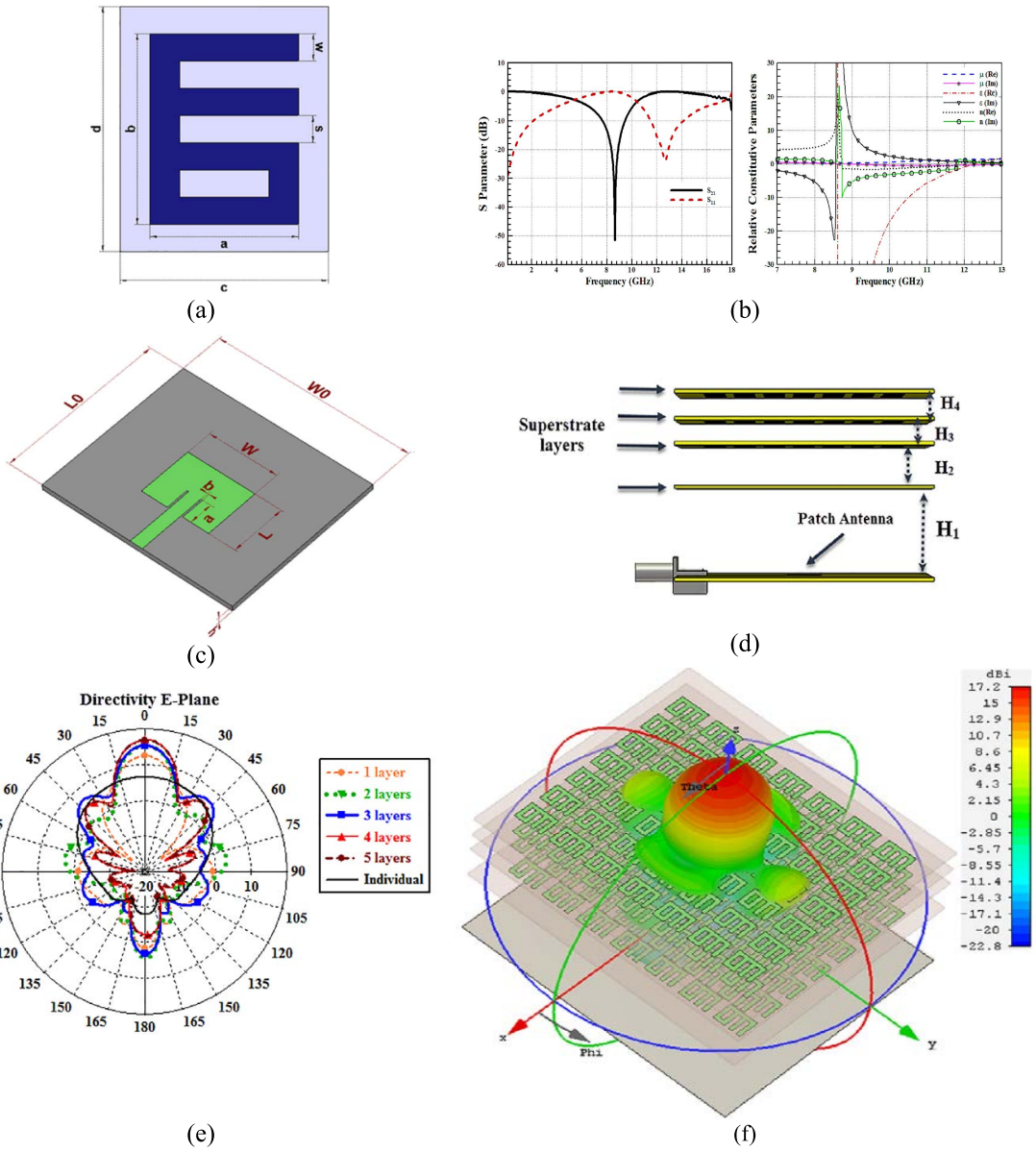

FIGURE 16. (a) Unit cell geometry. (b) Simulation set-up in CST studio. (c) Geometry of patch antenna. (d) Schematic of proposed antenna. (e) Antenna's directivity having different metamaterial layers along E-Plane. (f) 3D radiation model of proposed antenna [97] @ wiley.

1) RESULTS AND DISCUSSION

After simulating the unit cell in the CST microwave studio, the desired results fully satisfy the mu-negative characteristics. The unit cell has negative μ and positive ε values at the resonant frequency. The simulated results are shown in Fig.10.

To verify the negative μ and positive ε values mathematically, the Nicolson Rose Weir (NRW) method [94] is used. The procedure utilized by NRW method is deduced from the following equations:

$$X = \frac{S_{11}^2 - S_{21}^2 + 1}{2S_{11}} \tag{22}$$

The reflection coefficient is:

$$\Gamma = X \pm \sqrt{X^2 + 1} \tag{23}$$

The transmission coefficient will T be:

$$T = \frac{S_{11} + S_{21} - \Gamma}{1 - (S_{11} + S_{21})\Gamma} \tag{24}$$

$$1/\Lambda^2 = -\left[\frac{1}{2\pi L} ln(1/T)\right]^2 \tag{25}$$

The permeability is given as:

$$\mu_r = \frac{1 + \Gamma}{\frac{1}{\Lambda}(1 - \Gamma)\sqrt{1/\lambda_0^2 - 1/\lambda_c^2}} \tag{26}$$

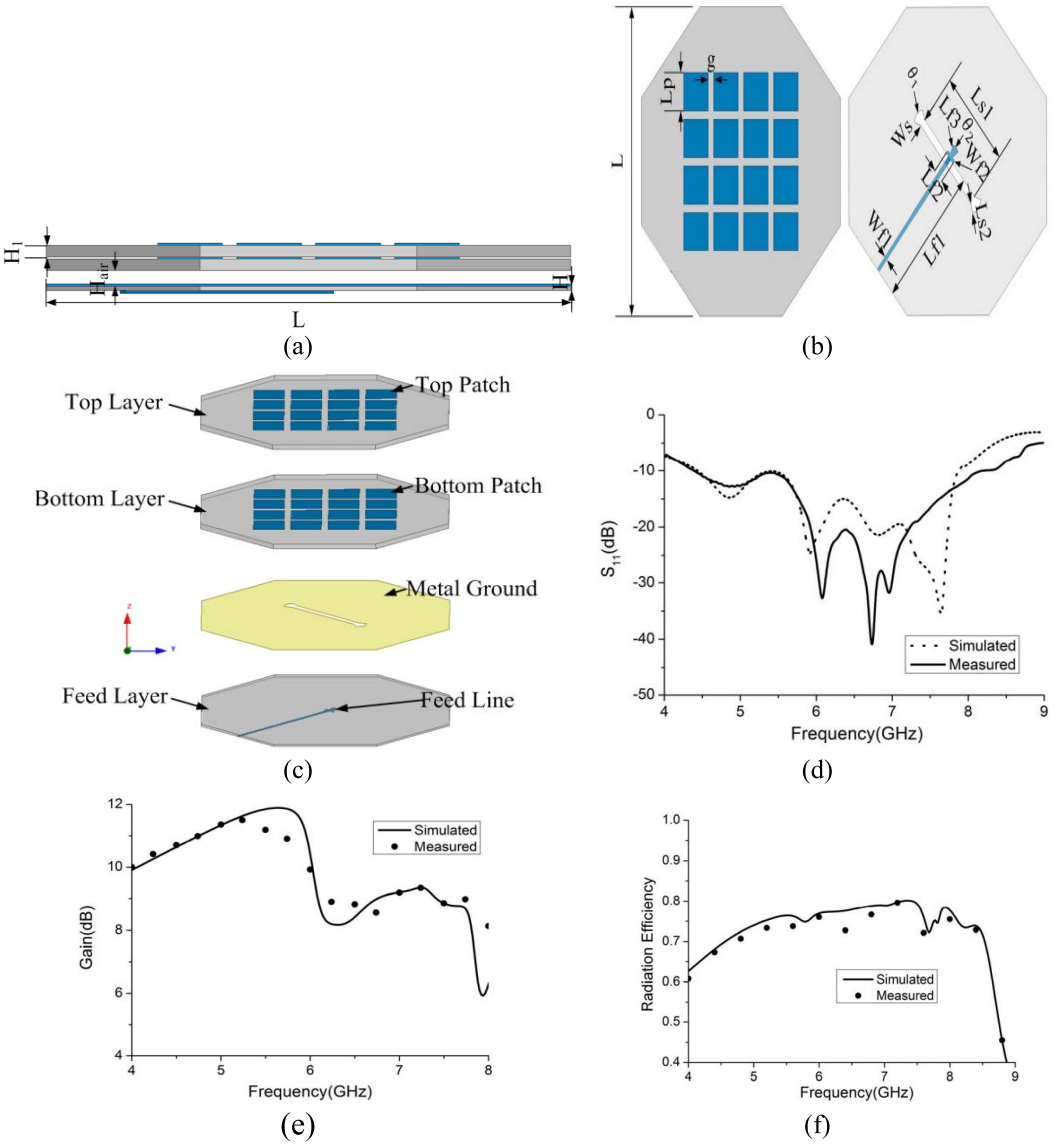

FIGURE 17. (a) Configuration of proposed antenna. Side and top view of the metasurface. (a) and (b) respectively. (c). Detailed structure of the proposed antenna. (d). Simulated and measured results of S_{11}. (e). Gain. (f). radiation efficiency of the proposed antenna [72] @IEEE.

The permittivity is given as:

$$\varepsilon_r = \frac{\lambda_0^2}{\mu_r}\left[\frac{1}{\lambda_c^2} - \frac{1}{2\pi L} ln(1/T)\right] \tag{27}$$

where λ_0 and λ_c are free-space and cut-off wavelengths respectively, while L is the sample's length. Using the above equations, the calculated values from NRW method for ε and μ are -7.88 and 2.13 respectively, thus verifying the simulations.

C. DNG BASED METASURFACES

The study on DNG property was first theorized in [9], and first practically demonstrated in [14]. To that end, a design was presented to achieve DNG characteristics by combining the thin wire-based ENG structure with the SRR-based MNG structure [15]. This combination satisfies the requirement of $\varepsilon < 0$ from a wire/rodded medium and $\mu < 0$ from a split ring resonator (SRR). In this paper, the same methodology is adopted and the unit cell which was designed for MNG material is considered with an edition of thin metallic wire at the backside of the substrate to fulfill the requirement of $\varepsilon < 0$, and few changes are made in design parameters to design DNG based metasurface. The geometry of the proposed unit cell is shown in Fig. 11. While Fig.12, shows the designed model in CST, and Table 3 provides parameter values of DNG based unit cell.

1) RESULTS AND DISCUSSION

The simulated results show that the desired DNG characteristics of the proposed design with negative μ and ε values are achieved, that is -3.01 and -0.7 respectively.

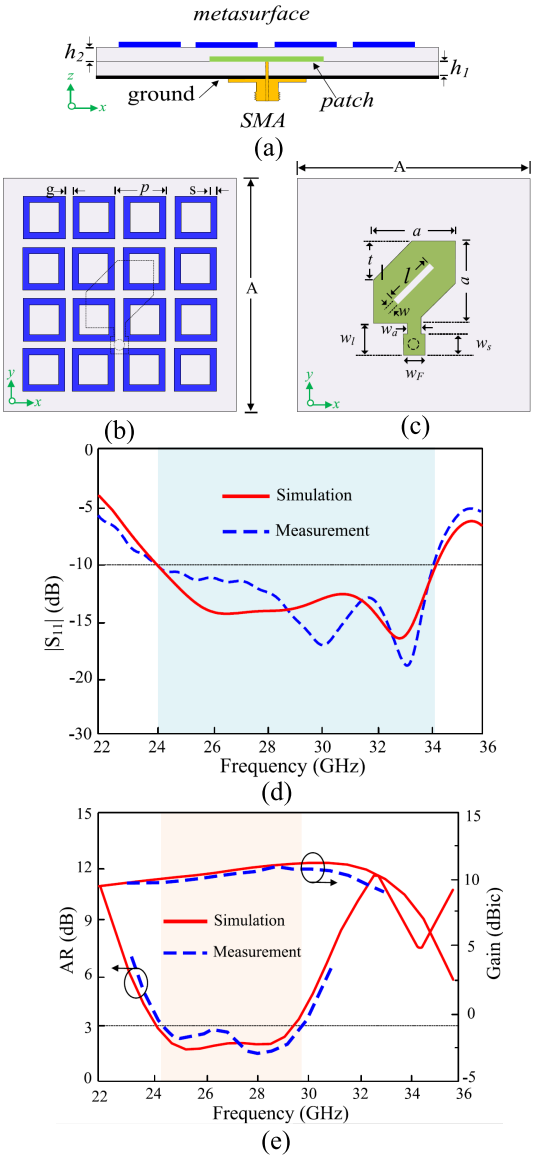

FIGURE 18. The geometry of the antenna proposed in [74], (a) Sideview, (b) top view of metasurface, (c) top view of the patch, (d) S-parameters, (e) Axial Ratio and Gain [74] @IEEE.

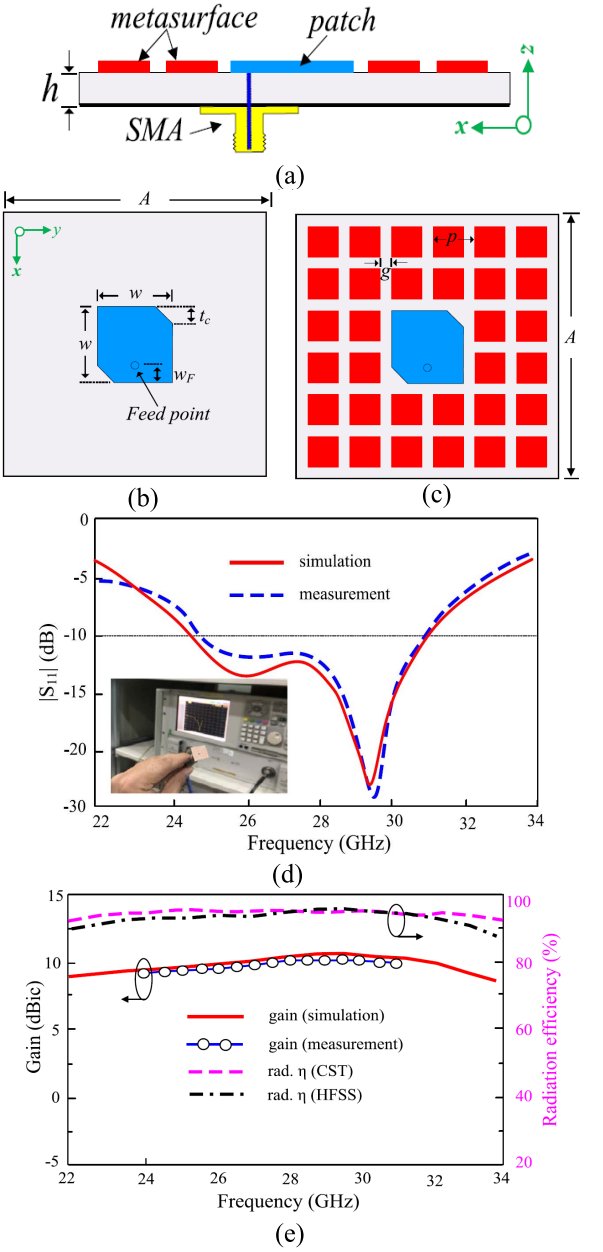

FIGURE 19. The geometry of the antenna proposed. (a) Sideview, (b) Top view of metasurface, (c) Top view of the patch, (d) S-parameters, (e) Gain and Radiation efficiency [75] @IEEE.

To verify the negative μ and ε values numerically, the NRW method [94] is again considered to calculate μ and ε values from the S-parameters, which come out as -4.36 and -5.1 respectively.

The metasurfaces are used in the literature to design antennas to achieve improved performance in terms of gain, bandwidth, beam steering, scanning, polarization, etc. The state-of-the-art vis-à-vis uses of different metasurfaces for improving antenna performance are discussed.

IV. STATE OF THE ART

A. GAIN AND DIRECTIVITY ENHANCEMENT

The gain enhancement of an antenna is related to other properties including improved radiation characteristics, high directivity, reduced surface waves, and back radiations [95]. According to Snell's law, when the refractive index of a material is negative (e.g., DNG materials), the waves converge twice, and the source image is created at two points which leads to an increase in the directivity and gain consequently [5], [6]. Considering the initial designing approach, a superstrate structure surrounded by the arrays of artificial magnetic conductors (AMCs) is placed above (or below) the radiating patch to enhance the antenna's gain, because when a metamaterial layer is used as a superstrate for a patch antenna it can increase both directivity and gain of the antenna [96]. Here it is important to mention that metamaterials are employed in antennas as artificial magnetic conductors (AMCs),

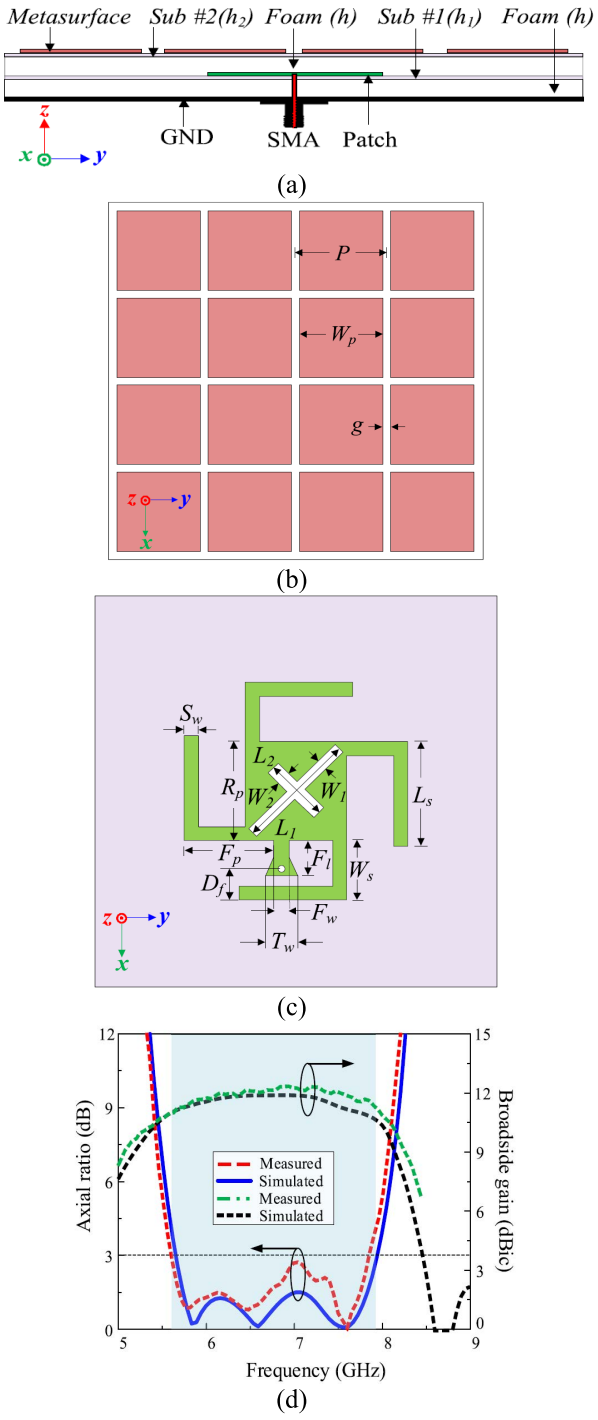

FIGURE 20. Geometry of prototype proposed in [98]. (a) Side-view, (b) Top-view of metasurface, (c) Top-view of patch, (d) Simulated and measured results [98] @IEEE.

because in AMCs, conductive current and the image current are in-phase, rather than out of phase. This implies that the reflection phase from AMC and PEC (perfect electric conductor) for a normal incident plane wave is equal to 0° and 180° respectively. And when these AMCs are incorporated into antennas, the structure act as a high-impedance surface (HIS) [1]. The scheme is shown in Fig. 14.

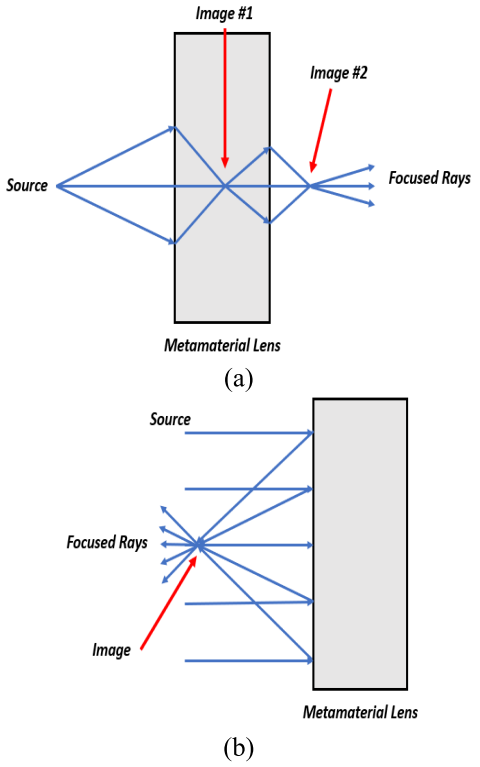

FIGURE 21. Waves refraction through NRI material. (a) Transmit-array focused lens, (b) Reflect-array focused lens [47] @Phys. Letters.

Adopting this concept, the Fabry-Pérot cavity model in [96] provides a high gain antenna of 14.1 dBi. In [96], the model was conceptualized by a metamaterial superstrate structure containing planar DNG metamaterials having a negative refractive index placed above the radiating patch resulting in 11.2 dBi of gain at 2.3 GHz frequency. The whole scheme is shown in Fig. 15.

Considering more significant gain enhancement led to antenna design in [97] as shown in Fig.16. The design contains more than one metamaterial-based superstrate layer above radiating patch to provide a strong guiding medium to the radiations which contributes to the significant gain enhancement of 17.1 dBi at 9.4 GHz.

Although the above-mentioned designs are good for increasing antenna's gain at the cost of increasing the size and thickness of antennas. Hence, these are not suitable for low-profile planar structures. Therefore, the prototypes in [72] and [73] and in [74] and [75] for 5G communications were reported to achieve high-gain antennas with miniaturized size. The proposed antenna in [72] has an octagon structure, metasurface with two-stacking layers, and ground plane. The excitation is done through a microstrip line and a slot etched on a ground plane. This design provides the maximum gain of 11.8 dBi over the variation of 1.7 dBi in the frequency range of 4.48 GHz-6.0 GHz, and 9.7 dBi with the variation of 1.5 dBi over the frequency range of 6.0 GHz-7.8 GHz. The antenna geometry and results are shown in Fig.17.

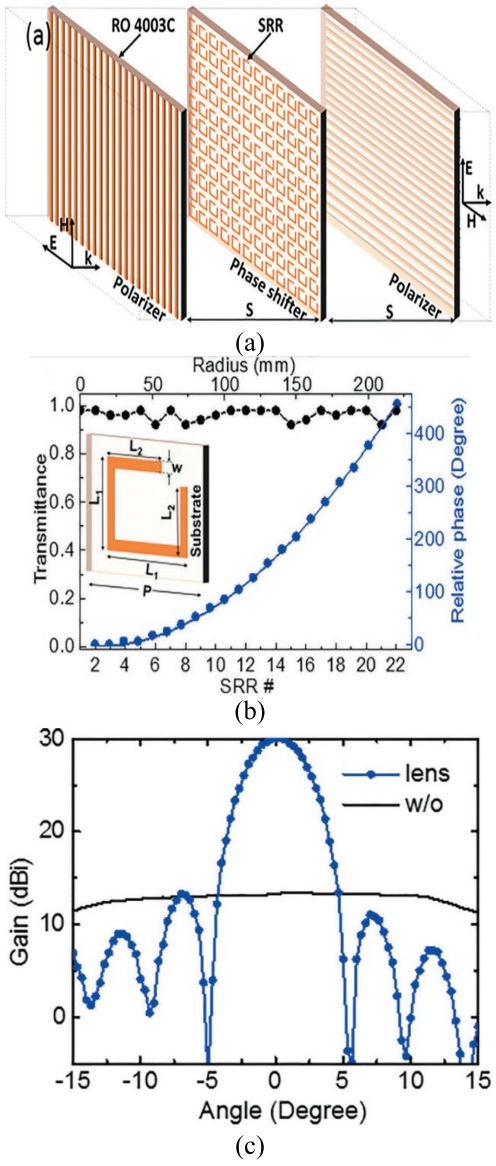

FIGURE 22. (a) Schematic representation of the proposed lens antenna, (b) Simulated transmittance and phase curves, (c) Measured gain for radiation from a horn with and without metasurface lens [80] @Phys. Letters.

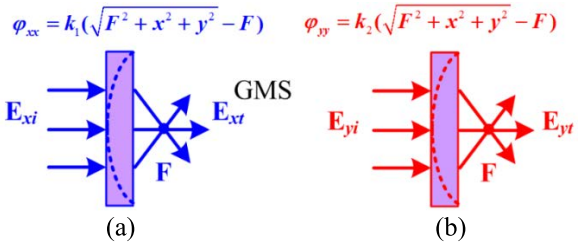

FIGURE 23. GMS operating at frequency f_1 (a) and f_2 (b) [81] @IEEE.

In technological innovation over time, this notion of gain enhancement was penetrated into 5G communications with a more low-profile design without an air gap between substrates, as illustrated in [74]. In [74], a metasurface containing square rings is stacked directly above a slotted radiating patch having truncated corners (for circular polarization) without air gap making the prototype low-profile for planar structures as shown in Fig.18. In this proposed scheme, metasurface act as high impedance surface, which supports in phase reflections i.e., at a resonance frequency of 27 GHz (this is the radiating patch frequency), the phase reflection of 0°, and ±90° from metasurface resulted in a wideband antenna of 24 – 34.1 GHz frequency with a maximum gain of 11 dBi and reduced size of $12 \times 12 \times 1.02\text{mm}^3$.

Further research investigation into this strategy led to the latest antenna design reported in [75], with an even smaller size having just a single substrate layer containing a radiating patch surrounded by a metasurface lattice of periodic patches. The configuration was being used to design an antenna having wide-bandwidth, single metasurface layer, low profile, circularly polarized characteristics, suitable for 5G mm-wave systems, and MIMO applications as shown in Fig.19. The antenna provides a high gain of 11 dBi over the wideband frequency range of 24.5 - 31 GHz, with a size of $12 \times 12 \times 0.51$ mm^3.

Similarly, for a lower frequency range, i.e., near 6 GHz, one of the noticeable works was presented in [98] for gain and bandwidth improvement. The proposed antenna in [98] consists of a patch antenna with a cross-slot for circular polarization and a simple square patch metasurface that excites multiple-resonances to improve the antenna's axial ratio up to 33.25% (5.64-7.89 GHz), along with gain and bandwidth up to 12.17 dBi and 65.06 % respectively, as shown in Fig.20.

B. LENS METASURFACES

Metamaterials owing negative refractive index properties are widely used as flat lens antennas which focus electromagnetic waves to increase directivity and gain. This unique feature amplifies and centralizes the evanescent and propagating ways in the materials which possess negative refractive index (NRI) [47]. For understating, Fig.21 presents the concept of lens metamaterial. Metamaterials act as transmit-array-focused lenses, to focus the waves at a single point in the forward direction. While metamaterials can also focus the rays in a backward direction through a reflect-array-focused lens.

Conventionally, for long-haul microwave communications, phase shifters were used as lens antennas for beam scanning objectives, which makes the design large, complex, and power-hungry for high data rate requirements. In the compensation, researchers came up with a new approach of lens metasurface antennas, which not only perform beam scanning operations more efficiently as compared to phased arrays system but also kept the design miniaturized and less power consumption. Hence, these metasurfaces-based lens antennas are highly applicable for collimating broadband microwaves both at transmit and reflect mode, beam steering, gain enhancement, radar cross-section reduction, broadband spectrum for 5G communication, and spatial beam forming for 5G and sub-6 GHz massive MIMO multi-beam systems.

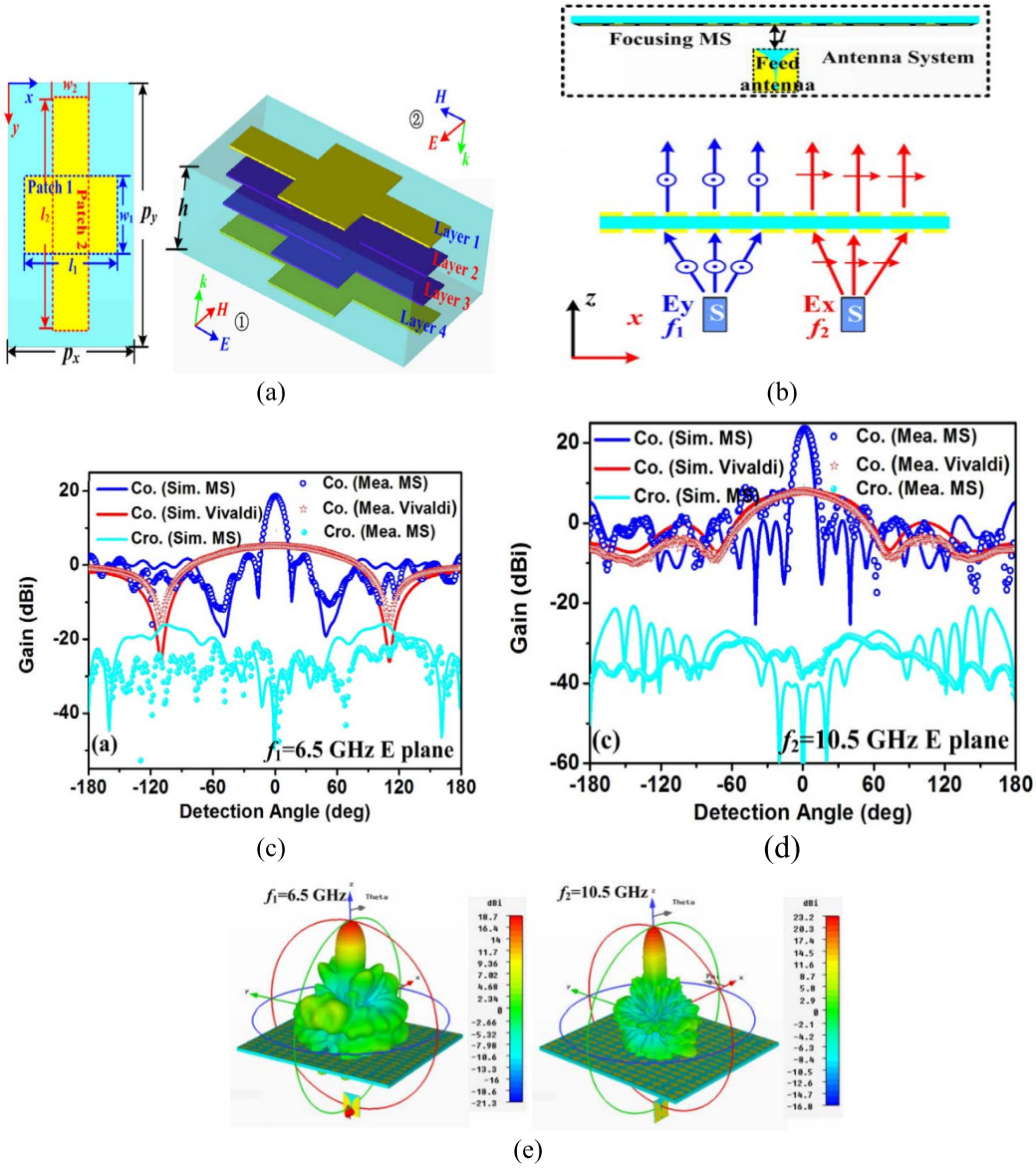

FIGURE 24. Topology of proposed antenna. (a) Top and sideview of unit cell, (b)Simulation model, (c) Radiation pattern for f_1 in xz-plane, (d) Radiation pattern for f_2 in yz-plane (d), (e) 3D radiation pattern [81] @IEEE.

As evident from Fig.21, that metasurface-based lens performance can be categorized in two ways i.e., transmit-array focused lens and reflect-array focused lens based on classified EM properties. There is a third category as well, which comprises the lens antennas performing both transmission and reflection functions simultaneously. All these categories are discussed below.

1) TRANSMITTER METASURFACE LENS ANTENNAS

To focus the incident EM waves transmitted from the horn feed antenna, metasurface-based lens antennas re-transmit the waves as the plane waves after the phase adjustment by phase shifter elements (i.e, unit cells). In [80] an ultra-thin, tri-layered metasurface-based planar lens contains 22 split rings resonators to collimate microwave beams in transmission mode at 9 GHz frequency with a gain of 17 dBi. Here the split ring resonator metasurface is sandwiched between metal grating which is perpendicularly oriented as shown in Fig.22. This resonator supports forward and backward cross- and co-polarized waves generating a highly focused transmissive beam with a gain of 17 dBi over the phase variation from 0 to 2.5π.

On the other hand, in [81] the dual-band transmissive gradient metasurface-based lens antenna for two operating bands i.e., C- and X-bands is presented. The model was designed to have a four-layer structure with the same structures at layers 1 and 4 and another same structure at layers 2 and 3 (naming it ABBA system) to obtain highly

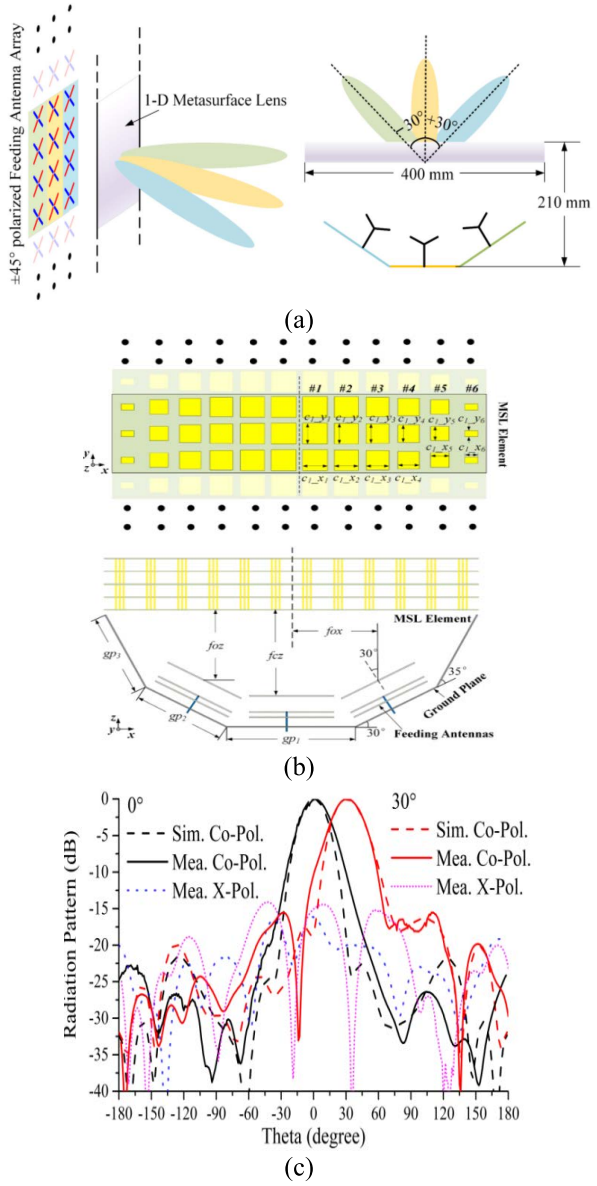

FIGURE 25. (a) Model schematics of multibeam lens antenna, (b) Deign configuration of the antenna, (c) Simulated and measured results at 1.17 GHz [82] @IEEE.

focused transmitted waves at both frequencies. After illuminating from different polarizers, gradient metasurface (GMS) operates at f_1 and f_2 with phase distributions of φ_{xx} and φ_{yy} respectively as:

$$\varphi_{xx} = k_1\left(\sqrt{F^2 + x^2 + y^2} - F\right) \tag{28}$$

$$\varphi_{yy} = k_2\left(\sqrt{F^2 + x^2 + y^2} - F\right) \tag{29}$$

The general schematic diagram of GMS is shown in Fig.23.

For the proposed design, under the different polarizers, GMS combines the incident waves of two lenses having the same focal length F at the frequencies $f_1$and f_2. There are two notable features of this design, first one is the two operating modes are highly isolated from each other due to

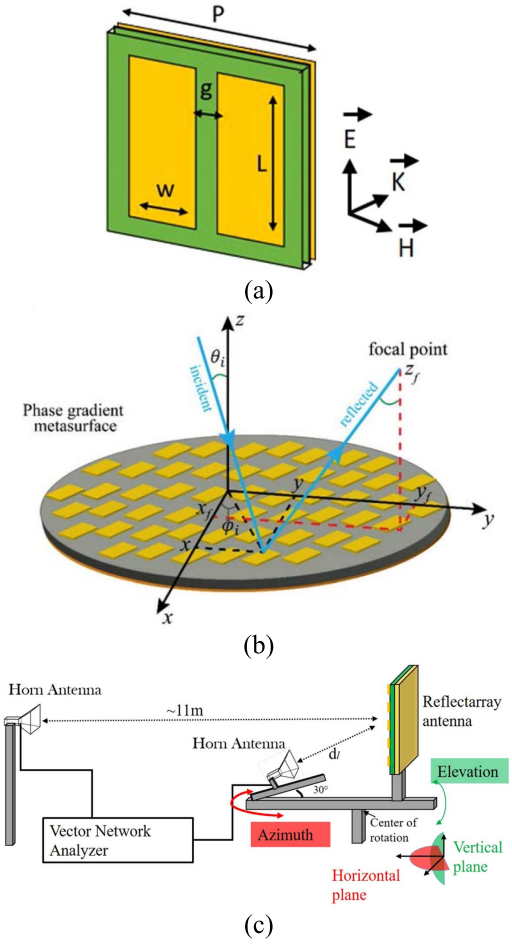

FIGURE 26. The geometry of proposed antenna. (a) Unit cell topology (a). (b) Metasurface reflect-array, (c) Working of fabricated model [83] @ Scientific Reports.

the perpendicular EM modes, and secondly, as EM waves are not interacting with each other, hence, the proposed antenna work efficiently at two operating bands resulting in highly directive beams of gain 18.7 dBi and 23 dBi for f_1 and f_2 respectively. The whole topology is shown in Fig.24.

In [82], the authors came up with a unique model to cater certain problems related to multi-beam lens antennas in microwave bands including small prototype size, low profile with no air gaps between substrate layers, wide bandwidth, dual-polarization, and low side-lobe levels (SLLs). Hence, it produced a novel prototype to provide a 5-layered metasurface-based reflectionless, wide bandwidth i.e., 1.71-2.2 GHz, multibeam (i.e., beams at 0° and ±30°), polarization-free lens antenna, with ±45° polarizer as the feeding antenna having the gain ranging from 10-13.5 dBi within ±30° coverage span. The results were verified for the beams at 0° and 30°. The schematics and results are shown in Fig.25.

2) REFLECTOR METASURFACE LENS ANTENNAS

As metasurface-based lens antennas focus the beams on transmissive mode, likewise, reflector metasurface lenses focus

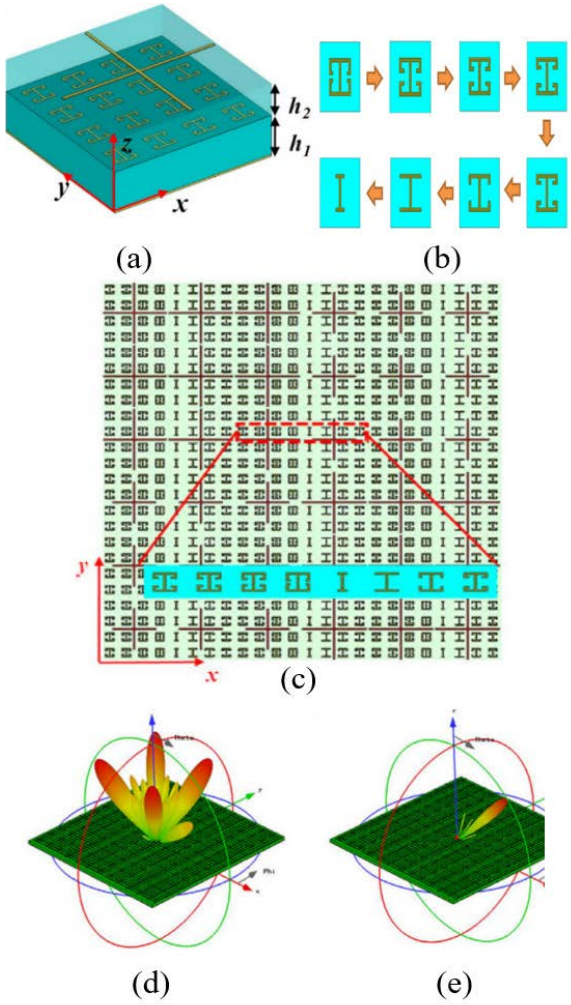

FIGURE 27. Schematics of proposed reflect-array metasurface lens. (a) Unit cell geometry, (b) I-shaped pattern, (c) Metasurface configuration, (d) 3D radiation pattern at 11 GHz, (e) and 25 GHz [84] @ Scientific Reports.

the beams on reflective mode. In reflector lenses, the ground is a must to prevent backward radiations. This methodology is best demonstrated by [83], in which a metasurface-based ultra-thin reflect-arrays lens is designed to perform beam collimation in reflected mode at 30° off-axis from the center to avoid interference issues with the feed antenna offering 27.5 dBi high gain at 11.8 GHz operating frequency. Moreover, the resonators that are employed in this prototype cover a phase range of 360°. The complete topology is shown in Fig. 26.

The same idea [84] also presents the reflect-array lens, but it is designed to administer a multi-spectral beam deflection and collimation at two different operating frequencies. In this design, the metasurface is composed of two-layered metallic patterns of different resonators, backed by a ground plane, i.e., the top layer contains a cross-line structure for developing phase response of reflected wave from 0° to 180°, while the bottom layer contains I-shaped patterns of topological morphing to devise gradient-phase distribution. Hence, reflected waves are being controlled freely, after being fed by the linear polarizer, and the model deflects the beams for the K-, X-, and Ku bands. Therefore, the design is capable to reduce radar cross-section efficiently. The schematics are shown in Fig. 27.

3) TRANSMIT AND REFLECT METASURFACE ANTENNAS

By combining the effects of DNG and MNG/ENG properties with the help of designed unit cells, a metasurface lens antenna can be devised which can transmit and reflect the incident waves. Therefore, the design proposed in [85] is analogous to this concept. In [85], a new bifunctional metasurface lens antenna was proposed to transmit and reflect incident waves (from the Vivaldi antenna feed source) simultaneously, by focusing x-polarized and y-polarized incident waves at the reflection and transmission side respectively, keeping focal length unchanged. This means that for the transmit array, the feed antenna is y-polarized and for the reflect array the feed antenna is rotated 90°, making it x-polarized. In addition, due to the rotation of the feed antenna, the reflect array can divert the beam at 147.5°, to prevent feed antenna blockage. The design consists of a 4-layered unit cell to cover a 360° phase span, with different geometry of cells for transmission and reflection purposes, as shown in fig.28. The antenna yields two highly directive beams for E//y (transmit-array) with the gain of 21.4 dBi and E//x (reflect-array) with the gain of 20 dBi at 10 GHz. The antenna's configuration and results are shown in Fig. 28.

Another very important trait of lens metasurface is the application for beam-scanning antenna used in 5G massive MIMO systems, demonstrated in [86]. It consists of a thin planar metasurface-based lens antenna containing two substrate layers with an air-gap having array of discrete unit cells for a phase shift to realize the multi-beam spatial beam-steering over the range of -27^{o} to $+27^{o}$. The feeding network consists of a stacked-patch, seven-element substrate integrated waveguide (SIW) antenna structure, which transmits and receives EM waves at the operating band of 28 GHz, backed by metal ground for the suppression of back-radiations as shown in Fig. 29. The prototype was designed by considering and properly addressing the three key challenges associated with the planar lens structures i.e., the gain and radiation efficiency should be high, minimum thickness of the structure, and the proper positioning of the focal arc, as it ensures the high gain throughout the scanning range. Hence, a suitable prototype for 5G massive MIMO systems having a high gain of 24.2 dBi, and beam-steering of $\pm 27^{o}$ range with stable radiations over the range of 26-29 GHz is proposed.

Adopting the same designing approach, the new metasurface lens antenna in [87] was designed to perform beam-steering for massive MIMO and multi-beam at the sub-6 GHz band (or 5G mm-wave band). The design is presented with some changes in the structure as compared to [86], like

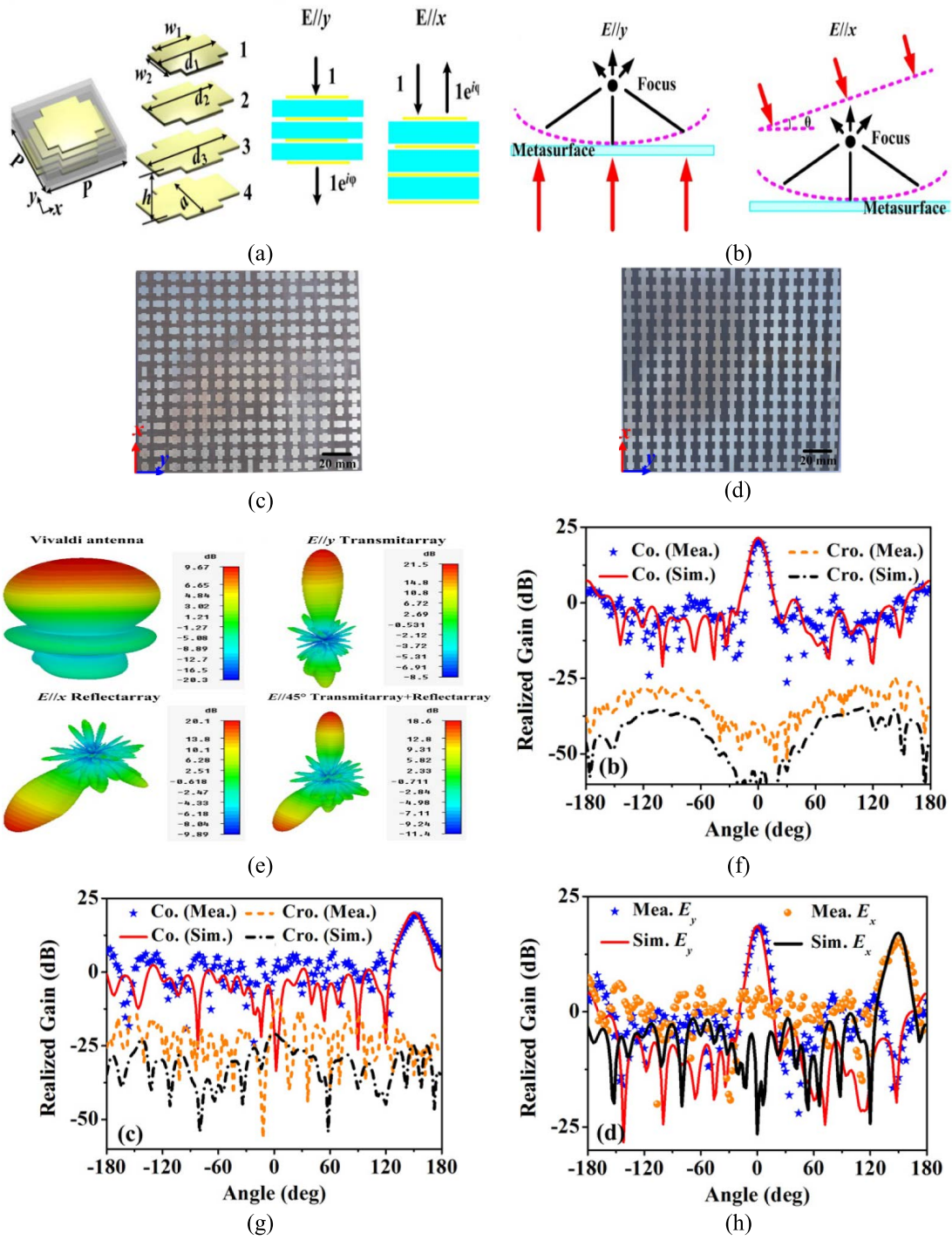

FIGURE 28. Lens Antenna Configuration [85]. (a) Schematics of unit cell, (b) Working topology of the lens excited by x- and y-polarized incident waves, (c) Top view and (d) bottom view of the metasuraface, (e) 3D radiation patterns, (f) Simulated and measured radiation pattern of proposed antenna transmit-array and (g) reflect-array and (h) combined transmit and reflect arrays of the proposed antenna [85] @IEEE.

the metasurface-based lens now composed of three substrate layers containing array unit cells to modify the phase of the incident and reflected waves as shown in Fig. 30. Moreover, the lens antenna is fed by stacked patch planar, 8 × 8 array structure to produce 64 dual-polarized beams, suggested for full dimension massive MIMO at 5G mm-wave band. Hence, the antenna with the desired characteristics of beam-steering within the range of $\pm 25^{o}$, producing a maximum gain of 22.4 dBi over the operating of 5.17-6.10 GHz is realized in [87].

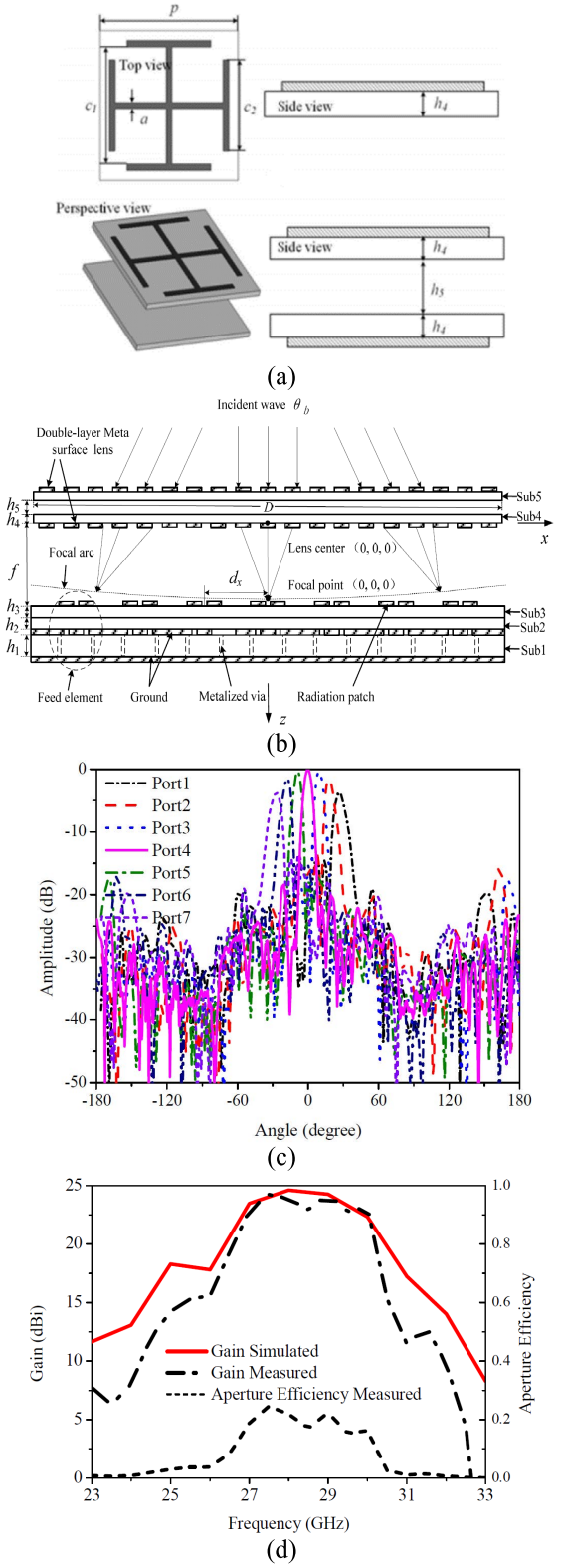

FIGURE 29. Configuration of the proposed antenna. (a) Top and perspective view of Jerusalem Cross (JC) unit cells for phase shifting, (b) Side-view of the metasurface lens loaded SIW fed elements, (c) Measured result of beam scanning at 28 GHz by the antenna, (d) Simulated and measured results of gain and aperture efficiency [86] @IEEE.

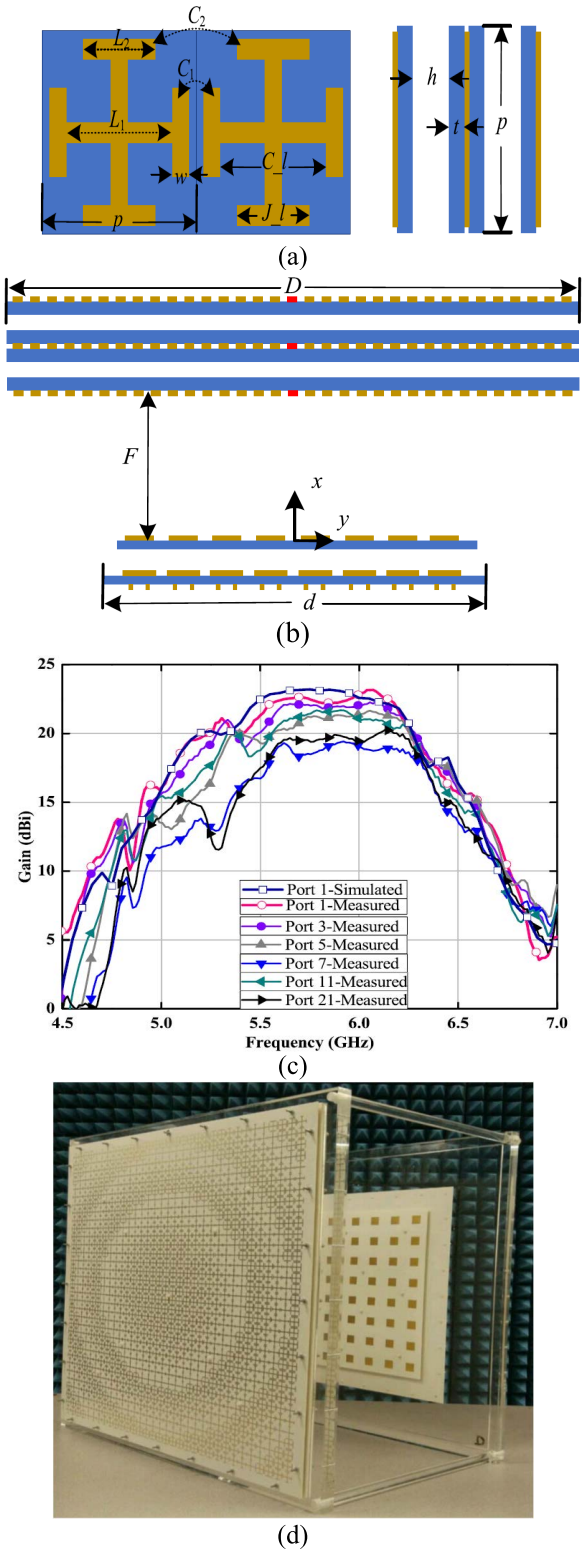

FIGURE 30. Architecture of proposed antenna. (a) Phase-shift Elements, (b) Configuration of lens and feeding structure, (c) Gain of proposed lens antenna feeding at different ports, (d) Fabricated prototype of the structure [87] @IEEE.

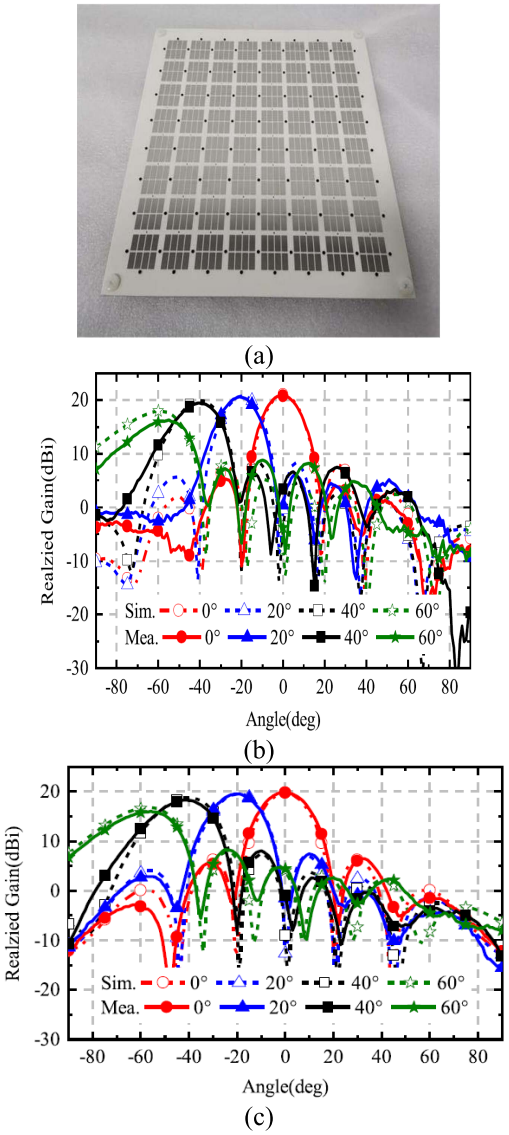

FIGURE 31. Prototype of 8 × 8 array structure at 5.4GHz (a), E-plane scanning pattern (b), H-plane scanning pattern (c) [99].

As it can be inferred, above mentioned beam scanning metasurfaces can't be incorporated for planar structures due to the large size and huge air gap between substrate layers. Hence, a novel topology was devised in [99], in which beam-scanning approach was conceptualized through a planar metasurface-based lens antenna. The prototype yields distinguishable results with $\pm 60^{o}$ beam-steering range, along with 22.2% impedance bandwidth and 21dBi gain of 8×8 array structure as shown in Fig. 31.

4) ABSORBER METASURFACES

The absorber antennas are highly demandable to avoid detection from radars. As it is stated before that by combining an ENG slab with an MNG slab, a perfect absorber antenna was designed and reported in [88] as shown in Fig. 32. The model consists of two resonators i.e., electric ring resonator

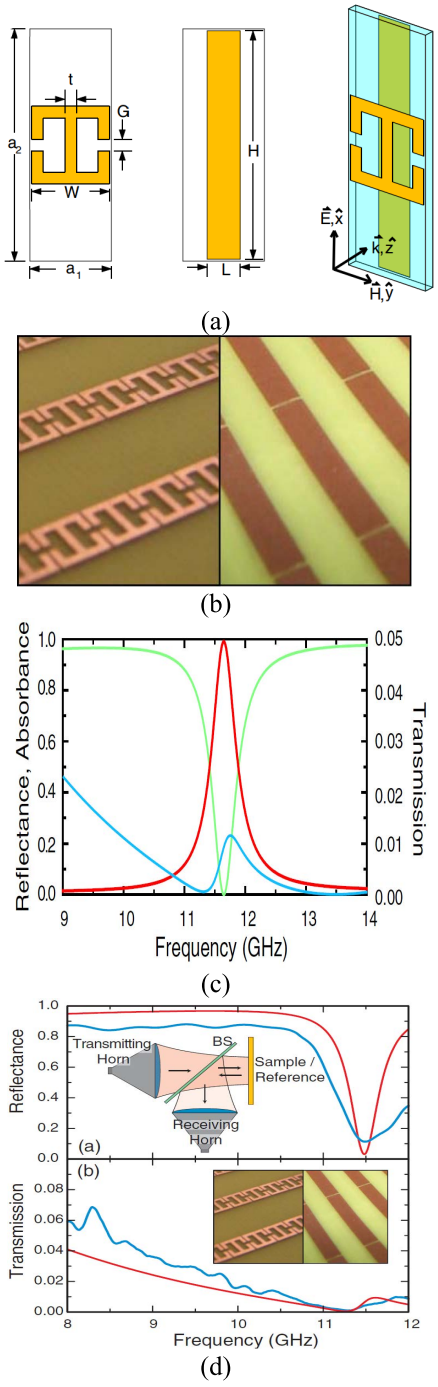

FIGURE 32. Configuration of proposed antenna. (a) Unit cell structure, (b) Metasurface structure, (c) Simulated results of unit cell absorber, (d) Simulated results of proposed.

to provide coupling and a metallic wire to provide magnetic coupling. Both resonators couple electric and magnetic fields separately to absorb incident waves completely, as the absorbance rate is unity. The antenna works at the operating frequency of 11.5 GHz.

The wideband absorbers are more in demand as compared to a single band. Therefore, [89] proposes an ultra-wideband

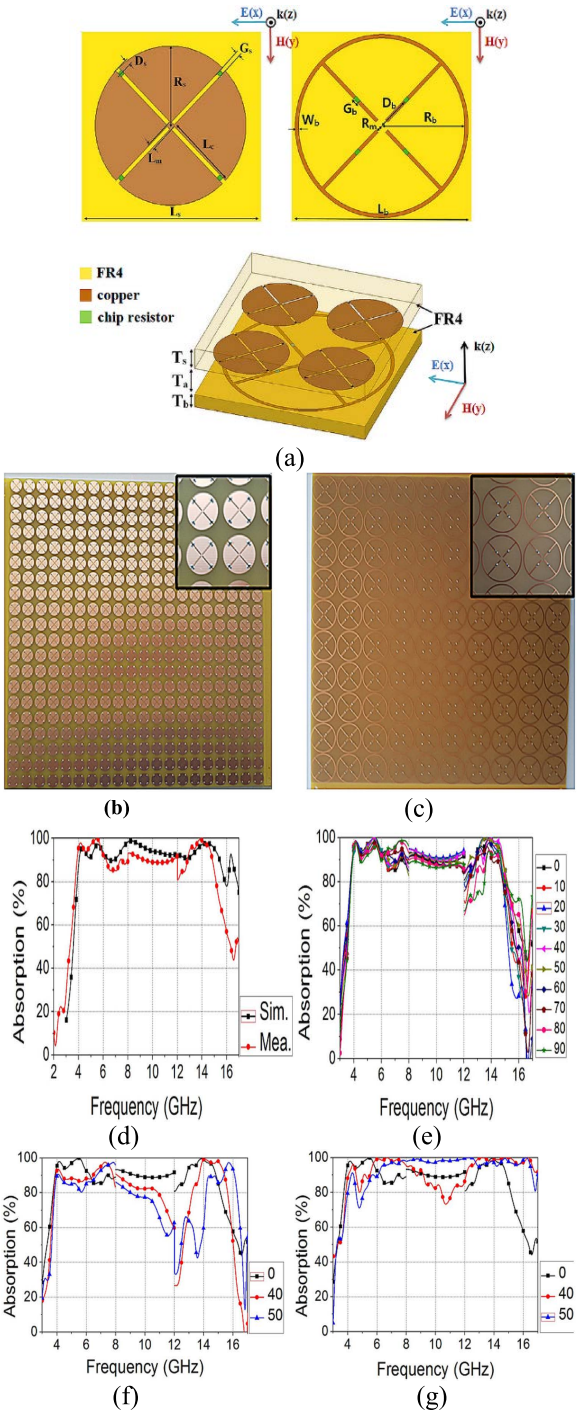

FIGURE 33. Topology of absorber metasurface proposed. (a) Unit cell configuration, (b) Top and (c) bottom view of metasurface, (d) Simulated and measured results of proposed absorber, (e) at different polarization angles, (f) for incident waves in TE mode (f), (g) for incident waves in TM mode [89] @IEEE.

metasurface-based absorber to meet the requirement. In [89], the absorber consists of two metasurfaces with different unit cell geometry in the upper and lower layers, with an air-gap between the layers. The model comprises three layers, where the upper layer contains unit cells having the geometry of the four complementary circular sectors to abate its coupling with the lower frequency metasurface. While the lower layer contains unit cells having the geometry of four symmetric circular sectors to diminish angle sensitivity and polarization, and the middle layer is with an air gap. To realize the broadband metasurface four chip resistors incorporate both unit cells. The performance of the proposed absorber was examined under normal and oblique incident angles, which shows that the absorber yields more than 90% absorbance in the range of 3.78-15.63 GHz for normal incident waves. While for oblique angles, it yields more than 80% absorbance under the transvers-electric (TE) mode with the strength of incident angle is as low as 40%, and the transverse-magnetic (TM) mode with strength of incident angle is as low as 50%. Hence, the model provides polarization insensitive absorber as shown in Fig.33.

As evident that the absorber metasurfaces are the perfect candidate for radar cross section reduction (RCSR), therefore, the model in [90] devised the hybrid-metasurface for mono-static and bi-static RCSR, which consists of anisotropic-frequency-selective-absorber i.e., AFS absorber and polarization-rotation-reflective-surface i.e., PR reflective surface. The co-polarized wave is absorbed by this AFS absorber, while the cross-polarized wave passes. Now the PR reflective surface, which is placed beneath the AFS absorber, a cross-polarized wave will be reflected with 90^{o} rotation and then it is absorbed by the AFS absorber. As the incident waves are being absorbed rather than deflected to other directions, both mono-static and bi-static RCSR is achieved in the frequency band ranging from 6 GHz to 8 GHz. The proposed configuration and results are shown in Fig. 34.

V. ANALYSIS ON THE EM-BASED CLASSIFIED METASURFACES

The analysis on the investigated research work described in this paper is presented in Table 4. As such the reported metasurface-based antennas in [72], [73], [74], and [75] were designed to achieve high gain with small size. Among these [74], [75] designs are designed for 5G communications with high gain and small size. The models proposed in [96] and [98] reveal that gain is enhanced by placing metasurface incorporated resonators in front (or on top) of radiating patch to direct the beams after passing through the structure. The gain achieved by [98] is much larger than that in [96] but at the cost of the antenna's size. The comparison between [74] and [75] reveals that the latter model is more suitable for low profile, a high gain antenna having just one substrate layer to ease the fabrication process as well. The examined antennas in [80], [81], [82], [83], [84], and [85] comprehend the concept of lens metasurfaces to design compact, high gain, and broad-band transmit and reflect antennas for beam-focusing. The presented metasurface antennas in [80], [81] behave as a transmit-array lens, which collimated the beam in the forward direction, but both designs didn't focus the waves at the specific point after passing through the metasurface. Similarly, the design in [82] also operates as

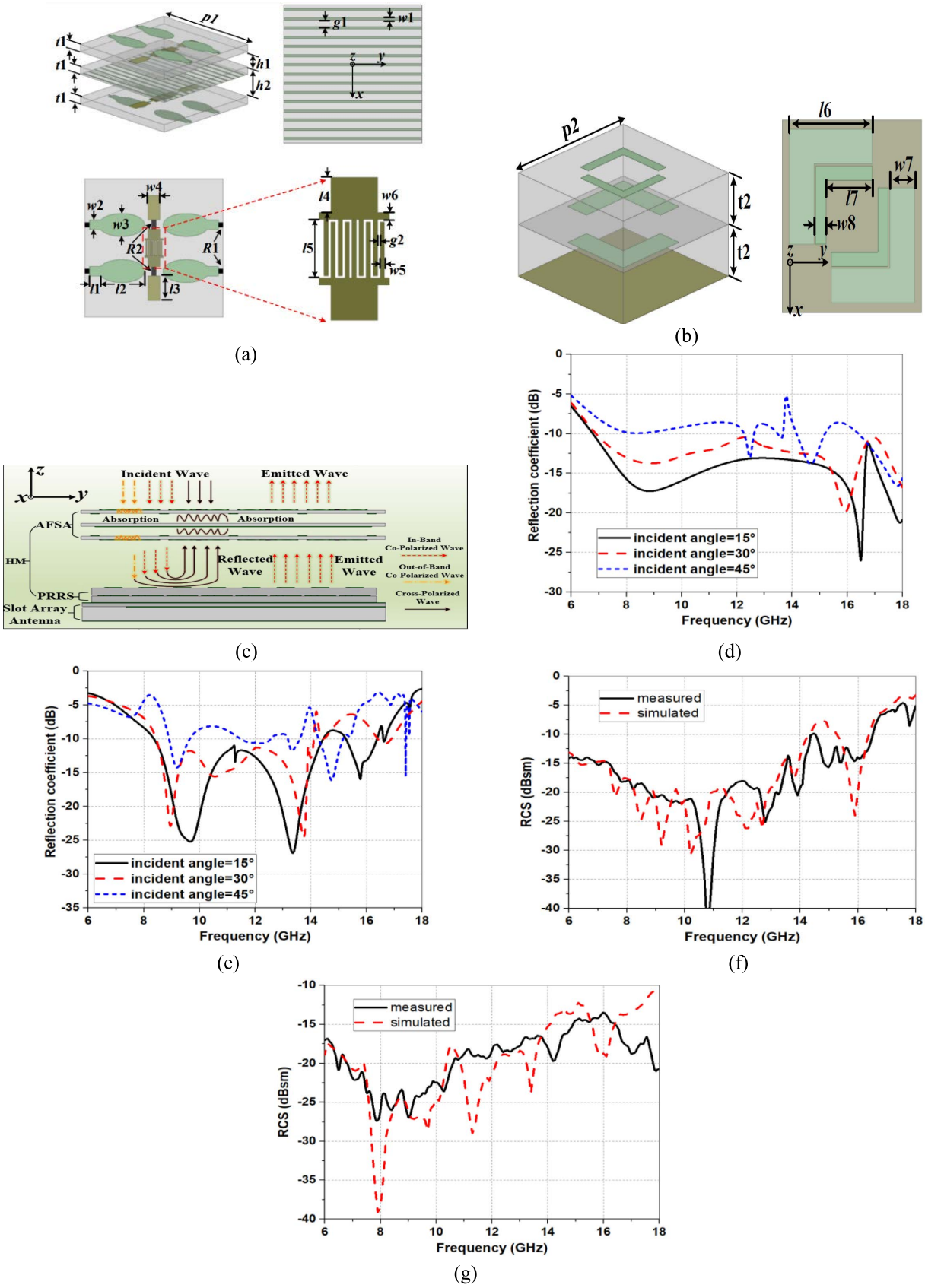

FIGURE 34. Geometry of absorber antenna proposed. (a) Unit cell for AFS absorber, (b) Unit cell for PR reflective surface, (c) Working methodology of proposed model (d) Reflection coefficients of metasurface for TE- (e) and TM-polarized incident wave, (f) The schematic results for mono-static RCSR of the antenna of x- polarized and (g) y-polarized incident wave [90] @IEEE.

TABLE 4. Analysis of the performance based on antenna types.

Sr. no.	Antenna Type	EM Classification	Application	Size (mm^3)	BW (GHz)	Max. Gain (dBi)
[72]	Multiple Superstrate MTS Antenna	DNG	Gain Enhancement + Wideband	102x102x8	4.48-7.87 6-7.87	11.8 9.7
[74]	Stack-packed MTS Antenna	DNG	High Gain + Wideband + Low profile	12x12x1.02	24-34.1	11
[75]	Single layered, MIMO MTS antenna	DNG	High Gain + Wideband + Low profile	12x12x0.51	24-34.1	11
[80]	Lens MTS Antenna	MNG/ENG	Beams focusing + Gain Enhancement	Not mentioned	7-10	17
[81]	Dualband Transmitted Lens MTS Antenna	MNG/ENG	Beams focusing + Gain Enhancement	Not mentioned	6.5 & 10.5	18.7 & 23
[82]	Broadband Transmitted Lens MTS Antenna	MNG/ENG	Multi-beam splitter lens	Not mentioned	1.71-2.2	10-13.5
[83]	Reflective Lens MTS	DNG	Gain Enhancement	440x440x60	11.8	27.5
[84]	Dual-band Reflective MTS	DNG	RCSR	7.4x11.2x1.6	11 & 25	Not mentioned
[85]	Transmit+Reflect array lens MTS	DNG + ENG/MNG	EM waves controller	20x20x6	10	21.4 (Tx) 20 (Rx)
[86]	Transmit+Reflect array lens MTS	DNG + ENG/MNG	Multi-beam phase shifter from ±27° for 5G	101.2x101.2 x50.6	28	24.2
[87]	Transmit+Reflect array lens MTS	DNG + ENG/MNG	Multi-beam phase shifter from ±27° for 5G mm-wave	50x50x25	5.17-6.10	22.4
[88]	MTS based Wireless Communication Prototype	ENG+MNG	MTS performs the function of phase-shifting for beamforming from 0°-60°	37x37x1	2.3 & 28.5	21.7 & 19.1
[89]	Electronically Steered MTS Antenna	ENG+MNG	Steers the beam in two directions i.e., azimuth (±50°) and elevation (±70°)	229x120x3.5	9-10.7	9.86
[90]	LC-Based Reflect-array MTS	DNG +ENG/MNG	Scan the beam with the range of ±40° for 6G	20x20x0.087	108	Not mentioned
[96]	Superstrate MTS Antenna	DNG	Gain Enhancement	262x262x73	2.3	11.2
[98]	Multiple Superstrate MTS Antenna	DNG	Gain Enhancement	40x28.7x41. 47	9.4-12	17.1
[99]	MTS based Beam scanning array	ENG	Scanning range of the beams is ±60° for sub-6GHz	196x196x3.8 61	4.8-6	21

a transmitted lens antenna but it yields multi-beam response. Contrarily, [83] and [84] act as reflect-array lens antennas to deflect and collimate the beam in a backward direction operating at single and multi-band frequencies. The need to attain both transmitted and reflected beam collimation from the single model is achieved by [85], [86], [87], but these are

complex designs, thus imposing difficulties in fabrications due to the multi-layered structure. The next regime is the absorber metasurfaces [90], [91], [92], which absorb all the incident waves either at a single operating frequency [90] or at a wide operating band [91], [92]. These designs are suitable candidates for radar cross-section reduction as well.

VI. CONCLUSION

In this paper, based on the electromagnetic classifications, a comprehensive overview with the help of designed metasurfaces unit cells, showing unique characteristics as ε-negative (ENG), μ-negative (MNG), and double negative (DNG) materials is demonstrated. First, the basic concept of materials with negative refractive index is demonstrated through Maxwell's equations. Then this concept is idealized by the unit cells to classify the material properties based on ε-negative, μ-negative, and double-negative parametric values. After that, the simulated results are further verified with the help of mathematical relations i.e., the Kramers-Krong and Nicolson Rose Weir (NRW) method. Moreover, state-of-the-art designs are discussed to highlight the utilization of classified metasurfaces for attaining the high gain metasurface-based antennas, lens metasurfaces for highly directive collimated beam antennas with compact antenna size both in transmitted (forward) and reflected (backward) modes and absorber antennas to reduce radar cross-section. A comparison of the state-of-the-art design is drawn to facilitate readers' understanding. In addition, based on the review, following recommendations are made: metasurfaces can be used for tackling the problem of circular polarization bandwidth enhancements, for providing beam scanning in millimeter wave band vis-à-vis 1-D or 2-D leaky wave antennas, and for designing shared aperture metasurface based antennas for both in microwave and millimeter wave bands.

REFERENCES

[1] M. Ben, *Metamaterials: Critique and Alternatives*. Hoboken, NJ, USA: Wiley, 2009.

[2] D. R. Smith, W. J. Padilla, D. C. Vier, S. C. Nemat-Nesser, and S. Schultz, "Composite medium with simultaneously negative permeability and permittivity," *Phys. Rev. Lett.*, vol. 84, p. 4184, May 2000.

[3] H.-T. Chen, A. J. Taylor, and N. Yu, "A review of metasurfaces: Physics and applications," *Rep. Prog. Phys.*, vol. 79, no. 7, Jul. 2016, Art. no. 076401.

[4] A. Sihvola, "Metamaterials in electromagnetics," *Metamaterials*, vol. 1, no. 1, pp. 2–11, Mar. 2007.

[5] W. J. Krzysztofik and T. N. Cao, "Metamaterials in application to improve antenna parameters," *Metamater. Metasurf.*, vol. 12, no. 2, pp. 63–85, 2018.

[6] C. Caloz and T. Itoh, *Electromagnetic Metamaterials: Transmission Line Theory and Microwave Applications: The Engineering Approach*. Hoboken, NJ, USA: Wiley, 2006.

[7] N. Engheta and R. W. Ziolkowski, *Metamaterials: Physics and Engineering Explorations*. Hoboken, NJ, USA: Wiley, 2006.

[8] G. V. Eleftheriades and K. G. Balmain, *Negative-Refraction Metamaterials: Fundamental Principle and Applications*. Hoboken, NJ, USA: Wiley, 2005, pp. 1–436.

[9] V. G. Veselago, "The electrodynamics of substances with simultaneously negative values of ϵ and μ," *Phys.-Uspekhi*, vol. 10, no. 4, pp. 509–514, 1968.

[10] R. W. Ziolkowski, "Design, fabrication, and testing of double negative metamaterials," *IEEE Trans. Antennas Propag.*, vol. 51, no. 7, pp. 1516–1529, Jul. 2003.

[11] N. Engheta and R. W. Ziolkowski, "A positive future for double-negative metamaterials," *IEEE Trans. Microw. Theory Techn.*, vol. 53, no. 4, pp. 1535–1556, Apr. 2005.

[12] A. Erentok, D. C. Vier, S. Schultz, R. W. Ziolkowski, J. A. Nielsen, R. B. Greegor, C. G. Parazzoli, M. H. Tanielian, A. S. Cummer, B.-I. Popa, and T. Hand, "Low frequency lumped element-based negative index metamaterial," *Appl. Phys. Lett.*, vol. 91, Oct. 2007, Art. no. 184104.

[13] G. V. Eleftheriades and K. G. Balmain, *Negative-Refraction Metamaterials: Fundamental Principles and Applications*. Hoboken, NJ, USA: Wiley, 2005.

[14] J. B. Pendry, A. J. Holden, D. J. Robbins, and W. J. Stewart, "Magnetism from conductors and enhanced nonlinear phenomena," *IEEE Trans. Microw. Theory Techn.*, vol. 47, no. 11, pp. 2075–2084, Nov. 1999.

[15] R. A. Shelby, D. R. Smith, S. C. Nemat-Nasser, and S. Schultz, "Microwave transmission through a two-dimensional, isotropic, left-handed metamaterial," *Appl. Phys. Lett.*, vol. 78, no. 4, pp. 489–491, Jan. 2001.

[16] E. Ozbay, K. Guven, and K. Aydin, "Metamaterials with negative permeability and negative refractive index: Experiments and simulations," *J. Opt. A, Pure Appl. Opt.*, vol. 9, no. 9, pp. S301–S307, Sep. 2007.

[17] K. B. Alici and E. Özbay, "Radiation properties of a split ring resonator and monopole composite," *Phys. Status Solidi (B)*, vol. 244, no. 4, pp. 1192–1196, Apr. 2007.

[18] I. K. Kim and V. V. Varadan, "Electrically small, millimeter wave dual band meta-resonator antennas," *IEEE Trans. Antennas Propag.*, vol. 58, no. 11, pp. 3458–3463, Nov. 2010.

[19] Y. D. Dong, T. Yang, and T. Itoh, "Substrate integrated waveguide loaded by complementary split-ring resonators and its applications to miniaturized waveguide filters," *IEEE Trans. Microw. Theory Techn.*, vol. 57, no. 9, pp. 2211–2223, Sep. 2009.

[20] H. Zhang, Y.-Q. Li, X. Chen, Y.-Q. Fu, and N.-C. Yuan, "Design of circular/dual-frequency linear polarization antennas based on the anisotropic complementary split ring resonator," *IEEE Trans. Antennas Propag.*, vol. 57, no. 10, pp. 3352–3355, Oct. 2009.

[21] A. U. Limaye and J. Venkataraman, "Size reduction in microstrip antennas using left-handed materials realized by complementary split-ring resonators in ground plane," in *Proc. IEEE Antennas Propag. Soc. Int. Symp.*, Jun. 2007, pp. 1869–1872.

[22] M. M. Bait-Suwailam and H. M. Al-Rizzo, "Size reduction of microstrip patch antennas using slotted complementary split-ring resonators," in *Proc. Int. Conf. Technolog. Adv. Electr., Electron. Comput. Eng. (TAEECE)*, May 2013, pp. 528–531.

[23] L. Yousefi and O. M. Ramahi, "Artificial magnetic materials using fractal Hilbert curves," *IEEE Trans. Antennas Propag.*, vol. 58, no. 8, pp. 2614–2622, Aug. 2010.

[24] D. Li, Z. Szabo, X. Qing, E.-P. Li, and Z. N. Chen, "A high gain antenna with an optimized metamaterial inspired superstrate," *IEEE Trans. Antennas Propag.*, vol. 60, no. 12, pp. 6018–6023, Dec. 2012.

[25] J. Naqui and F. Martín, "Angular displacement and velocity sensors based on electric-LC (ELC) loaded microstrip lines," *IEEE Sensors J.*, vol. 14, no. 4, pp. 939–940, Apr. 2014.

[26] V. Rawat, V. Nadkarni, and S. N. Kale, "ISM (industrial scientific and medical standard) band flex fuel sensor using electrical metamaterial device," *Appl. Phys. A, Solids Surf.*, vol. 123, no. 1, pp. 1–4, Jan. 2017.

[27] O. M. Khan, Z. U. Islam, Q. U. Islam, and F. A. Bhatti, "Multiband high-gain printed Yagi array using square spiral ring metamaterial structures for S-band applications," *IEEE Antennas Wireless Propag. Lett.*, vol. 13, pp. 1100–1103, 2014.

[28] G. Du and C. Liu, "Multiband metamaterial structure: Butterfly-pattern resonator," *Microw. Opt. Technol. Lett.*, vol. 54, no. 9, pp. 2179–2181, Sep. 2012.

[29] C. Zhu, J. J. Ma, H. Q. Zhai, L. Li, and C. H. Liang, "Characteristics of electrically small spiral resonator metamaterial with electric and magnetic responses," *IEEE Antennas Wireless Propag. Lett.*, vol. 11, pp. 1580–1583, 2012.

[30] O. Yurduseven, G. Turhan-Sayan, and A. E. Yilmaz, "Hybrid-shaped single-loop resonator: A four-band metamaterial structure," *Electron. Lett.*, vol. 47, no. 25, pp. 1381–1382, Dec. 2011.

[31] O. Turkmen, E. Ekmekci, and G. Turhan-Sayan, "Nested U-ring resonators: A novel multi-band metamaterial design in microwave region," *IET Microw., Antennas Propag.*, vol. 6, no. 10, pp. 1102–1108, Jul. 2012.

[32] S. U. Afsar, M. R. I. Faruque, M. J. Hossain, M. U. Khandaker, H. Osman, and S. Alamri, "Modified hexagonal split ring resonator based on an epsilon-negative metamaterial for triple-band satellite communication," *Micromachines*, vol. 12, no. 8, p. 878, Jul. 2021.
[33] E. Ekmekci and G. Turhan-Sayan, "Single loop resonator: Dual-band magnetic metamaterial structure," *IET Electron. Lett.*, vol. 46, no. 5, pp. 324–325, 2010.
[34] D. Marathe and K. Kulat, "A compact triple-band negative permittivity metamaterial for C, X-band applications," *Int. J. Antennas Propag.*, vol. 2017, pp. 1–12, Jan. 2017.
[35] O. Borazjani, M. N. Moghadasi, J. R. Mohassel, and R. A. Sadeghzadeh, "Design and analysis of a new wide-band epsilon negative metamaterial for X-band applications," *IETE J. Res.*, pp. 1–11, Jul. 2020, doi: 10.1080/03772063.2020.1792357.
[36] J.-H. Park, Y.-H. Ryu, and J.-H. Lee, "Mu-zero resonance antenna," *IEEE Trans. Antennas Propag.*, vol. 58, no. 6, pp. 1865–1875, Jun. 2010.
[37] J.-H. Park, Y.-H. Ryu, J.-G. Lee, and J.-H. Lee, "Epsilon negative zeroth-order resonator antenna," *IEEE Trans. Antennas Propag.*, vol. 55, no. 12, pp. 3710–3712, Dec. 2007.
[38] A. Dhouibi, S. N. Burokur, A. D. Lustrac, and A. Priou, "Low-profile substrate-integrated lens antenna using metamaterials," *IEEE Antennas Wireless Propag. Lett.*, vol. 12, pp. 43–46, 2013.
[39] M. Luo, X. Sang, J. Tan, and J. Chen, "A novel miniaturized metamaterial lens antenna," *Int. J. RF Microw. Comput.-Aided Eng.*, vol. 30, no. 7, Jul. 2020, Art. no. e22219.
[40] M. Puentes, M. Maasch, M. Schubler, and R. Jakoby, "Frequency multiplexed 2-dimensional sensor array based on split-ring resonators for organic tissue analysis," *IEEE Trans. Microw. Theory Techn.*, vol. 60, no. 6, pp. 1720–1727, Jun. 2012.
[41] A. Sabban, "New compact wearable metamaterials circular patch antennas for IoT, medical and 5G applications," *Appl. Syst. Innov.*, vol. 3, no. 4, p. 42, Oct. 2020, doi: 10.3390/asi3040042.
[42] D. Schurig, J. J. Mock, B. J. Justice, S. A. Cummer, J. B. Pendry, A. F. Starr, and D. R. Smith, "Metamaterial electromagnetic cloak at microwave frequencies," *Science*, vol. 314, no. 5801, pp. 977–980, Nov. 2006.
[43] F. Bilotti, A. Toscano, K. B. Alici, E. Ozbay, and L. Vegni, "Design of miniaturized narrowband absorbers based on resonant-magnetic inclusions," *IEEE Trans. Electromagn. Compat.*, vol. 53, no. 1, pp. 63–72, Feb. 2011.
[44] J. Yang and Z. Shen, "A thin and broadband absorber using double-square loops," *IEEE Antennas Wireless Propag. Lett.*, vol. 6, pp. 388–391, 2007.
[45] Y. Liu and X. Zhao, "Perfect absorber metamaterial for designing low-RCS patch antenna," *IEEE Antennas Wireless Propag. Lett.*, vol. 13, pp. 1473–1476, 2014.
[46] A. Grbic and G. V. Eleftheriades, "Overcoming the diffraction limit with a planar left-handed transmission-line lens," *Phys. Rev. Lett.*, vol. 92, no. 11, Mar. 2004, Art. no. 117403.
[47] J. B. Pendry, "Negative refraction makes a perfect lens," *Phys. Rev. Lett.*, vol. 85, no. 18, pp. 3966–3969, Oct. 2000.
[48] A. Grbic and G. V. Eleftheriades, "Experimental verification of backward-wave radiation from a negative refractive index metamaterial," *J. Appl. Phys.*, vol. 92, no. 10, pp. 5930–5935, Nov. 2002.
[49] B. A. F. Esmail, H. A. Majid, Z. Z. Abidin, S. H. Dahlan, and M. K. A. Rahim, "Reconfigurable metamaterial structure at millimeter wave frequency range," *Int. J. Electr. Comput. Eng. (IJECE)*, vol. 7, no. 6, p. 2942, Dec. 2017.
[50] Z. M. Zhang and C. J. Fu, "Unusual photon tunneling in the presence of a layer with a negative refractive index," *Appl. Phys. Lett.*, vol. 80, no. 6, pp. 1097–1099, Feb. 2002.
[51] L. Wu, S. He, and L. Chen, "On unusual narrow transmission bands for a multilayered periodic structure containing left-handed materials," *Opt. Exp.*, vol. 11, pp. 1283–1290, Jun. 2003.
[52] R. W. Ziolkowski and A. D. Kipple, "Application of double negative materials to increase the power radiated by electrically small antennas," *IEEE Trans. Antennas Propag.*, vol. 51, no. 10, pp. 2626–2640, Oct. 2003.
[53] A. Sanada, M. Kimura, I. Awai, C. Caloz, and T. Itoh, "A planar zeroth-order resonator antenna using a left-handed transmission line," in *Proc. 34th Eur. Microw. Conf.*, 2004, pp. 1341–1344.
[54] M. A. Antoniades and G. V. Eleftheriades, "A folded-monopole model for electrically small NRI-TL metamaterial antennas," *IEEE Antennas Wireless Propag. Lett.*, vol. 7, pp. 425–428, 2008.
[55] Y. Dong and T. Itoh, "Miniaturized substrate integrated waveguide slot antennas based on negative order resonance," *IEEE Trans. Antennas Propag.*, vol. 58, no. 12, pp. 3856–3864, Dec. 2010.
[56] T. Jang, J. Choi, and S. Lim, "Compact coplanar waveguide (CPW)-fed zeroth-order resonant antennas with extended bandwidth and high efficiency on via less single layer," *IEEE Trans. Antennas Propag.*, vol. 59, no. 2, pp. 363–372, Feb. 2011.
[57] Y. Dong, H. Toyao, and T. Itoh, "Compact circularly-polarized patch antenna loaded with metamaterial structures," *IEEE Trans. Antennas Propag.*, vol. 59, no. 11, pp. 4329–4333, Nov. 2011.
[58] Z. Xu, Q. Zhang, and L. Guo, "A compact 5G decoupling MIMO antenna based on split-ring resonators," *Int. J. Antennas Propag.*, vol. 2019, pp. 1–10, Jun. 2019, doi: 10.1155/2019/3782528.
[59] K. Jairath, N. Singh, V. Jagota, and M. Shabaz, "Compact ultrawide band metamaterial-inspired split ring resonator structure loaded band notched antenna," *Math. Problems Eng.*, vol. 2021, pp. 1–12, May 2021.
[60] R. Selvaraju, M. H. Jamaluddin, M. R. Kamarudin, J. Nasir, and M. H. Dahri, "Complementary split ring resonator for isolation enhancement in 5G communication antenna array," *Prog. Electromagn. Res. C*, vol. 83, pp. 217–228, Apr. 2018, doi: 10.2528/pierc18011019.
[61] X. Lai, Q. Li, P.-Y. Qin, B. Wu, and C.-H. Liang, "A novel wideband band-pass filter based on complementary split-ring resonator," *Prog. Electromagn. Res. C*, vol. 1, pp. 177–184, Feb. 2008, doi: 10.2528/pierc08013104.
[62] R. Li, Q. Zhang, Y. Kuang, X. Chen, Z. Xiao, and J. Zhang, "Design of a miniaturized antenna based on split ring resonators for 5G wireless communications," in *Proc. Cross Strait Quad-Regional Radio Sci. Wireless Technol. Conf. (CSQRWC)*, Jul. 2019, pp. 1–4.
[63] M. K. Ishfaq, T. A. Rahman, H. T. Chattha, and M. Ur Rehman, "Multi-band split-ring resonator based planar inverted-F antenna for 5G applications," *Int. J. Antennas Propag.*, vol. 2017, pp. 1–7, Mar. 2017, doi: 10.1155/2017/5148083.
[64] A. Dadgarpour, M. S. Sorkherizi, and A. A. Kishk, "High-efficient circularly polarized magnetoelectric dipole antenna for 5G applications using dual-polarized split-ring resonator lens," *IEEE Trans. Antennas Propag.*, vol. 65, no. 8, pp. 4263–4267, Aug. 2017.
[65] Z. Wang, Y. Dong, and T. Itoh, "Miniaturized wideband CP antenna based on metaresonator and CRLH-TLs for 5G new radio applications," *IEEE Trans. Antennas Propag.*, vol. 69, no. 1, pp. 74–83, Jan. 2021.
[66] P.-N. Choubey, W. Hong, Z.-C. Hao, P. Chen, T.-V. Duong, and J. Mei, "A wideband dual-mode SIW cavity-backed triangular-complimentary-split-ring-slot (TCSRS) antenna," *IEEE Trans. Antennas Propag.*, vol. 64, no. 6, pp. 2541–2545, Jun. 2016.
[67] T. P. Weldon, K. Miehle, R. S. Adams, and K. Daneshvar, "A wideband microwave double-negative metamaterial with non-foster loading," in *Proc. IEEE Southeastcon*, Mar. 2012, pp. 1–5.
[68] S. S. Islam, M. T. Islam, and M. R. I. Faruque, "A new wideband double negative metamaterial," in *Proc. IEEE 12th Malaysia Int. Conf. Commun. (MICC)*, Nov. 2015, pp. 319–322.
[69] Y. J. Huang, G. J. Wen, T. Q. Li, and K. Xie, "Low-loss, broadband and tunable negative refractive index metamaterial," *J. Electromagn. Anal. Appl.*, vol. 2, no. 2, pp. 104–110, 2010.
[70] A. Mahmood, G. O. Yetkin, and C. Sabah, "Wideband negative permittivity and double negative fishnet-mushroom-like metamaterial in X-band waveguide," *Adv. Condens. Matter Phys.*, vol. 2017, pp. 1–7, Feb. 2017.
[71] M. Hasan, M. Faruque, S. Islam, and M. Islam, "A new compact double-negative miniaturized metamaterial for wideband operation," *Materials*, vol. 9, no. 10, p. 830, Oct. 2016.
[72] H. Bai, G.-M. Wang, and T. Wu, "High-gain wideband metasurface antenna with low profile," *IEEE Access*, vol. 7, pp. 177266–177273, 2019.
[73] C. Zhao and C.-F. Wang, "Characteristic mode design of wide band circularly polarized patch antenna consisting of H-shaped unit cells," *IEEE Access*, vol. 6, pp. 25292–25299, 2018.
[74] N. Hussain, M. Jeong, A. Abbas, T. Kim, and N. Kim, "A metasurface-based low-profile wideband circularly polarized patch antenna for 5G millimeter-wave systems," *IEEE Access*, vol. 8, pp. 22127–22135, 2020.
[75] N. Hussain, M. Jeong, A. Abbas, and N. Kim, "Metasurface-based single-layer wideband circularly polarized MIMO antenna for 5G millimeter-wave systems," *IEEE Access*, vol. 8, pp. 130293–130304, 2020.
[76] Y. M. Pan, P. F. Hu, X. Y. Zhang, and S. Y. Zheng, "A low-profile high-gain and wideband filtering antenna with metasurface," *IEEE Trans. Antennas Propag.*, vol. 64, no. 5, pp. 2010–2016, May 2016.
[77] W. E. I. Liu, Z. N. Chen, X. Qing, J. Shi, and F. H. Lin, "Miniaturized wideband metasurface antennas," *IEEE Trans. Antennas Propag.*, vol. 65, no. 12, pp. 7345–7349, Dec. 2017.
[78] S. X. Ta and I. Park, "Compact wideband circularly polarized patch antenna array using metasurface," *IEEE Antennas Wireless Propag. Lett.*, vol. 16, pp. 1932–1936, 2017.

[79] S. X. Ta and I. Park, "Planar, high-gain, wideband, circularly polarized metasurface-based antenna array," *J. Electromagn. Waves Appl.*, vol. 30, no. 12, pp. 1620–1630, Jul. 2016.
[80] A. K. Azad, A. V. Efimov, S. Ghosh, J. Singleton, A. J. Taylor, and H.-T. Chen, "Ultra-thin metasurface microwave flat lens for broadband applications," *Appl. Phys. Lett.*, vol. 110, no. 22, May 2017, Art. no. 224101.
[81] T. Cai, G. Wang, J. Liang, Y. Zhuang, and T. Li, "High-performance transmissive meta-surface for C-/X-band lens antenna application," *IEEE Trans. Antennas Propag.*, vol. 65, no. 7, pp. 3598–3606, Jul. 2017.
[82] T. Li and Z. N. Chen, "Compact wideband wide-angle polarization-free metasurface lens antenna array for multibeam base stations," *IEEE Trans. Antennas Propag.*, vol. 68, no. 3, pp. 1378–1388, Mar. 2020.
[83] S. R. Silva, A. Rahman, W. D. M. Kort-Kamp, J. J. Rushton, J. Singleton, A. J. Taylor, D. A. R. Dalvit, H.-T. Chen, and A. K. Azad, "Metasurface-based ultra-lightweight high-gain off-axis flat parabolic reflectarray for microwave beam collimation/focusing," *Sci. Rep.*, vol. 9, no. 1, pp. 1–7, Dec. 2019.
[84] C. Huang, W. Pan, X. Ma, and X. Luo, "Multi-spectral metasurface for different functional control of reflection waves," *Sci. Rep.*, vol. 6, no. 1, pp. 1–7, Mar. 2016.
[85] T. Cai, G.-M. Wang, X.-L. Fu, J.-G. Liang, and Y.-Q. Zhuang, "High-efficiency metasurface with polarization-dependent transmission and reflection properties for both reflectarray and transmitarray," *IEEE Trans. Antennas Propag.*, vol. 66, no. 6, pp. 3219–3224, Jun. 2018.
[86] M. Jiang, Z. N. Chen, Y. Zhang, W. Hong, and X. Xuan, "Metamaterial-based thin planar lens antenna for spatial beamforming and multi-beam massive MIMO," *IEEE Trans. Antennas Propag.*, vol. 65, no. 2, pp. 464–472, Feb. 2017.
[87] S. Li, Z. N. Chen, T. Li, F. H. Lin, and X. Yin, "Characterization of metasurface lens antenna for Sub-6 GHz dual-polarization full-dimension massive MIMO and multibeam systems," *IEEE Trans. Antennas Propag.*, vol. 68, no. 3, pp. 1366–1377, Mar. 2020.
[88] N. Landy, S. Sajuyigbe, J. Mock, D. Smith, and W. Padilla, "Perfect metamaterial absorber," *Phys. Rev. Lett.*, vol. 100. no. 20, 2008, Art. no. 207402.
[89] D. Lim and S. Lim, "Ultrawideband electromagnetic absorber using sandwiched broadband metasurfaces," *IEEE Antennas Wireless Propag. Lett.*, vol. 18, no. 9, pp. 1887–1891, Sep. 2019.
[90] Y. Liu, Y. Jia, W. Zhang, and F. Li, "Wideband RCS reduction of a slot array antenna using a hybrid metasurface," *IEEE Trans. Antennas Propag.*, vol. 68, no. 5, pp. 3644–3652, May 2020.
[91] J. B. Pendry, A. J. Holden, D. J. Robbins, and W. J. Stewart, "Low frequency plasmons in thin-wire structures," *J. Phys. Condens. Matter*, vol. 10, no. 22, pp. 4785–4809, Jun. 1998.
[92] Z. Szabo, G.-H. Park, R. Hedge, and E.-P. Li, "A unique extraction of metamaterial parameters based on Kramers–Kronig relationship," *IEEE Trans. Microw. Theory Techn.*, vol. 58, no. 10, pp. 2646–2653, Oct. 2010.
[93] O. Sydoruk, E. Tatartschuk, E. Shamonina, and L. Solymar, "Analytical formulation for the resonant frequency of split rings," *J. Appl. Phys.*, vol. 105, no. 1, Jan. 2009, Art. no. 014903.
[94] R. Schwarz, "Measurement of material dielectric properties," Version 5, Rohde & Schwarz, Columbia, MD, USA, Tech. Rep. RAC0607-0019_1_4E, May 2012.
[95] P. K. Singh, J. Hopwood, and S. Sonkusale, "Metamaterials for remote generation of spatially controllable two dimensional array of microplasma," *Sci. Rep.*, vol. 4, no. 1, pp. 1–5, May 2015.
[96] D. Kim and J. Choi, "Analysis of antenna gain enhancement with a new planar metamaterial superstrate: An effective medium and a Fabry-Pérot resonance approach," *J. Infr., Millim., Terahertz Waves*, vol. 31, no. 11, pp. 1289–1303, Nov. 2010.
[97] O. Borazjani, M. Naser-Moghadasi, J. Rashed-Mohassel, and R. Sadeghzadeh, "Design and fabrication of a new high gain multilayer negative refractive index metamaterial antenna for X-band applications," *Int. J. RF Microw. Comput.-Aided Eng.*, vol. 30, no. 9, Sep. 2020, Art. no. e22284.
[98] K. E. Kedze, H. Wang, and I. Park, "A metasurface-based wide-bandwidth and high-gain circularly polarized patch antenna," *IEEE Trans. Antennas Propag.*, vol. 70, no. 1, pp. 732–737, Jan. 2022.
[99] Y. Li and S. Xiao, "Wideband wide-angle scanning phased array based on miniaturized metasurface antenna," *IEEE Trans. Antennas Propag.*, vol. 70, no. 2, pp. 1107–1119, Feb. 2022.

KOMAL IQBAL received the B.S. degree in electronics engineering from the University of Engineering and Technology, Taxila, Pakistan, in 2018. She is currently pursuing the master's degree in electrical engineering with the Department of Electrical Engineering, College of Electrical and Mechanical Engineering, CEME, NUST, Pakistan. Her research interests include wireless communication and metasurface-based antenna design. She was a recipient of the Scotland Pakistan Scholarships for Young Women and Girls (master's/M.phil).

QASIM UMAR KHAN (Member, IEEE) received the B.E. and M.S. degrees in computer systems and electrical engineering from the College of E&ME, National University of Sciences and Technology (NUST), Pakistan, in 2009 and 2011, respectively, and the Ph.D. degree in electrical engineering from NUST. He is currently serving as an Associate Professor at NUST. He has worked on antenna projects including MIMO antenna design for millimeter wave applications shared aperture antenna for sub 6 GHz and millimeter wave applications. Currently, he is working on high gain wideband circularly polarized metasurface based antenna and a low-cost wide-angle beam scanning SIW leaky wave metasurface-based antenna. He has published over 50 articles in many reputed journals and conference. His research interests include digital communication and digital signal processing, planar antenna designs, microwave devices, metasurfaces-based antennas, and leaky wave antennas. He was awarded with Best Teacher and Best Community Service Awards. He was also a recipient of the Undergraduate Scholarship of his university.